Search for antideuteron signal with AMS-02 detector in space

Mariusz Sapinski [*], Simonetta Gentile

INFN Sezione di Roma

P.le Aldo Moro, 2

00185 Roma

November 21, 2007

Abstract

AMS-02 is a large acceptance magnetic spectrometer which will be installed on the International Space Station. It will provide the most precise measurements of charged cosmic rays in energy range from 1 GeV up to a few TeV. One of the components of cosmic rays are antideuterons. Their contribution to the total flux is estimated to be around 10^{-11} and they have never been detected. A significant part of the low energy antideuteron flux might originate from Dark Matter annihilation and it is considered as one of the most background-free signatures of the Galactic Dark Matter halo. This study is performed to evaluate the AMS-02 sensitivity for antideuteron flux and contains a proposition of analysis strategy.

[*]mail: mariusz.sapinski@cern.ch

Contents

1 Introduction

This study reveals the capability of the AMS-02 experiment to detect antideuterons ($\bar{\text{d}}$) in cosmic rays. Despite of many essays [1, 2] no $\bar{\text{d}}$ in cosmic rays has ever been registered. The best limit on $\bar{\text{d}}$ flux has been obtained by BESS balloon experiment [1, 3] and is equal to $1.9 \cdot 10^{-4}$ [$\text{m}^{-2}\,\text{s}^{-1}\,\text{sr}^{-1}\,\text{GeV}^{-1}$] in the kinetic energy range $E_k = 0.17 - 1.15$ GeV/nucleon.

AMS-02 is a large-acceptance magnetic spectrometer designed to collect cosmic rays during a three-year flight onboard the International Space Station (ISS). Due to large acceptance and long data taking period it will be the most sensitive charged cosmic ray detector ever constructed. Therefore AMS-02 creates an unique opportunity to detect $\bar{\text{d}}$ in cosmic rays.

The antideuteron detection is important for two main reasons. First, it would provide an additional constraint for models of cosmic ray production and propagation in the Galaxy. According to these models the secondary production of cosmic rays results in production of small amounts of antideuterons in processes like $\text{p}_{\text{CR}}+\text{N}_{\text{ISM}} \rightarrow \bar{\text{d}} + \text{X}$ or $\text{p}_{\text{CR}} + \bar{\text{p}}_{\text{ISM}} \rightarrow \bar{\text{d}} + \text{X}$, where N_{ISM} and $\bar{\text{p}}_{\text{ISM}}$ are nuclei and antiprotons in Inter-Stellar Medium and p_{CR} are cosmic ray protons. On the left plot of Figure 1 an expected flux of antideuterons from secondary production is compared with fluxes of other cosmic ray components. The value of $\bar{\text{d}}$ flux is about 10^{-7} [$\text{m}^{-2}\,\text{s}^{-1}\,\text{sr}^{-1}\,\text{GeV}^{-1}$] in the kinetic energy range from 1 to 10 GeV/nucleon and is well below the fluxes of the main cosmic ray components.

The second reason of importance of $\bar{\text{d}}$ search is the possibility that a part of the flux might originate from Dark Matter annihilation [4] and the $\bar{\text{d}}$ signal could be an evidence of Dark Matter halo in Galaxy. On the right plot of Figure 1 an example of an expected $\bar{\text{d}}$ flux in the Earth proximity is presented. The red line represents flux from annihilation of neutralinos (χ^2) in a favorable supersymmetric model with parameters[1] $m_0 = 300$ GeV, $m_{1/2} = 450\ GeV$ and $\tan\beta = 50$ (model L from [6], $m_\chi = 190$ GeV). The profile of halo used to generate this flux is Navarro-Frenk-White [7] with the local halo density 0.3 GeV/cm^3. The $\bar{\text{d}}$ from background processes (ie. secondary $\bar{\text{d}}$) are marked with a black line. The most promising region for Dark Matter search is for kinetic energies below 1 GeV/nucleon, where the background from standard processes is negligible.

The goals of these study are the following:

- Determine the analysis strategy (ie. set of selection criteria and event-reconstruction procedures) to identify antideuteron events and reject backgrounds.

- Estimate the AMS-02 sensitivity to standard and supersymmetric antideuteron flux.

---

[1]Explanation of the supersymmetric parameters can be found in many overviews of Supersymmetry for example [5]
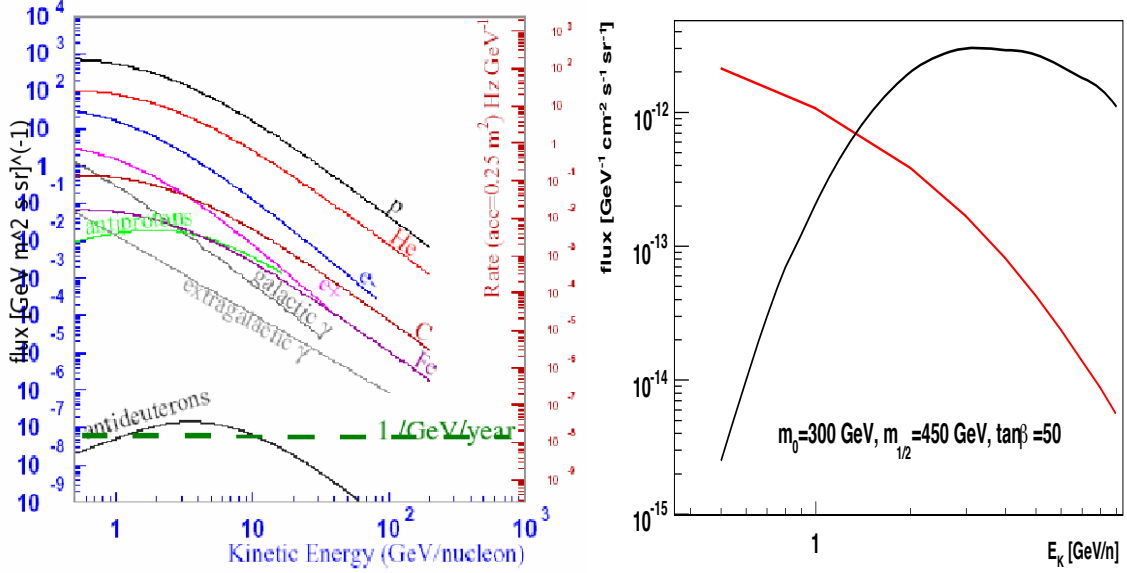
Figure 1: *Left plot: comparison of fluxes of various cosmic ray components. Right plot: comparison of secondary $\bar{\mathrm{d}}$ flux with signal from Supersymmetric Dark Matter annihilation in $\bar{\mathrm{d}}$ channel. Red line represents antideuteron flux as a function of kinetic energy per nucleon for SUGRA model as estimated by DarkSUSY [8] and SUSPECT [9] programs (model L - see text). Antideuterons from standard secondary production are represented by black line [4].*

The note is organized as follows. In the Section 2 the methods and specific aspects of the analysis are discussed. In the Section 3 the informations about the Monte Carlo samples used in the analysis are presented. The Section 4 is devoted to presentation of preselection requirements. It is followed by the estimation of geometrical acceptance in the Section 5 and by the Sections 6 which describes the analysis cuts. The final results, including an estimation of accessible Supersymmetry parameter space, are presented in the Section 7.

2   Methodology

A shortage of data on antideuteron interaction with matter and specific construction of the AMS-02 detector are the two issues important for this particular analysis.

The official version of GEANT [10] package, which is used to simulate interactions in the detector, does not contain the description of the interactions of antideuterons with matter. These interactions have been introduced in a special, tailored version of GEANT [11].

4

In order to test this implementation a comparative study with use of deuterons and antimatter correction coefficient has been made. This correction coefficient has been obtained from comparison of selection efficiencies for protons and antiprotons. The precision of this method is limited because the correction which is made is global, ie. it does not take into account the way the different selection criteria are sensitive to use of matter instead of antimatter.

The first phase of the study is the estimation of AMS-02 geometrical acceptance to antideuterons. For this purpose both approaches (antideuterons and deuterons with antimatter correction factor) have been used in order to obtain a comparison.

The second phase of the study is determination of the optimal set of analysis requirements in order, to isolate the antideuteron sample. This is a challenging procedure due to very limited expected statistics.

The parameters used to select $\bar{d}$ are mass and charge, therefore the mass and charge resolution are crucial. Mass resolution depends on momentum (p) and velocity (β) resolutions:

$$\frac{\delta m}{m} = \frac{\delta p}{p} \oplus \gamma^2 \frac{\delta \beta}{\beta} \tag{1}$$

Where momentum is measured by Silicon Tracker and velocity is measured by Time of Flight detector (TOF) or Ring Imaging Cherenkov (RICH) detector. Both detectors perform differently and are effective in different energy ranges.

The measurement based on RICH detector is characterized by a better precision than TOF, but for the radiator used in AMS-02 the Cerenkov radiation is emitted by particles with momenta higher than 6 GeV/c. In the same time the TOF measurement becomes imprecise for such energies because of limited time resolution of TOF readout. Above momenta of 6 GeV/c the RICH acceptance is approximately 80% of the total AMS acceptance.

As a consequence of such setup for velocity measurement, in this analysis the RICH velocity is used whenever possible, ie. whenever RICH velocity is available and passes the selection. In other cases the TOF measurement is used.

The electric charge of the particles is measured from energy deposits in TOF, tracker and RICH and its sign from direction of the bending of the particle track in magnetic field. The charge confusion is lower than 10^{-8} for particles with Z=1 at low kinetic energy.

The cosmic ray electrons are about 10^8 times more abundant than antideuterons. It is possible to achieve a good rejection against this background using TRD measurements. The selection in TRD also helps to choose events with small scattering in TRD, ie. events with reconstructed momentum close to the generated/real one (see Section 6.4.3).

Protons, deuterons and antiprotons constitute a large backgrounds in the antideuteron search. The protons are the most abundant component of cosmic rays. Their contribution to the total flux is about 10^{11} times larger than the antideuterons. The rejection of protons makes use of mass criteria and sign of charge determination.

The deuteron component is about 10^8 larger than the antideuteron one. Deuteron rejection can relay only on sign of charge determination. As mentioned above the sign-of-charge confusion is lower than 10^{-8} which is enough to reject deuteron background.

The antiproton component of the cosmic rays is about 10^6 larger than the antideuteron one. The rejection of antiprotons is based only on the mass criteria and they constitute the most important reducible background for the antideuteron search.

3 Event generation

Three types of the Monte Carlo events have been used in the analysis. Two of them are used by the two methods of acceptance estimation (see Section 5). The third kind of events has been used to optimize the analysis selection (see Section 6).

The first type of events, used for estimation of acceptance, is based on deuteron sample and uses antimatter correction obtained from proton and antiproton samples. The primary particles are generated from the inner surface of the box with dimensions $(3.9 \times 3.9 \times 3.9 \text{ m}^3)$ placed around the AMS-02 detector. They are generated with fixed momentum values between 0.9 and 30 GeV/c. The sample does not belong to the official AMS Monte Carlo production[2], but has been generated with use of the AMS-02 simulation software.

In the second approach the antideuterons itself have been used to calculate the acceptance. The particles in the sample are generated only on the top plane of the box surrounding the AMS-02 detector. This way of generation, instead of generation on the all surfaces of the box, leads to a systematic uncertainty on geometrical acceptance, but only this sample of antideuterons has been available. The momentum values of primary particles are: 1, 2, 4, 8 and 16 GeV/c. The acceptance has been calculated for antideuterons, antiprotons and electrons. This sample is a part of the official AMS Monte Carlo production (year 2005).

The third kind of the Monte Carlo events has been used to optimize the efficiency of the antideuteron selection and background rejection. These events are generated, as before, from the top surface of the box around the AMS-02. Particles are generated with a spectrum constant in logarithm of momentum (ie. power law spectrum with approximate index -2.6) and in momentum range between 0.5 and 10 GeV/c. In case of deuterons and antideuterons the momentum range is between 0.5 and 20 GeV/c, in order to keep the same range of kinetic energy per nucleon. This spectrum has been chosen in order to approach the real situation, where a typical power-law spectrum of cosmic rays will be measured.

All Monte Carlo samples contain only the events which pass Level 1 trigger conditions (LVL1) [12]. Typically the efficiency to pass LVL1 criteria, for an event generated on the surface of the box surrounding the AMS-02, is about 1%.

The summary of the Monte Carlo samples used in the final analysis is presented

---

[2]The production database is under URL: `http://pcamss0.cern.ch/mm.html`

in Table 1. The first column describes the particle type, the second shows the momentum range, the third one translates momentum into kinetic energy per nucleon. In the last column the number of generated particles is quoted in case of the acceptance studies (the first and the second type) and in case of antideuteron selection algorithm study this column contains the number of events passing LVL1 trigger conditions.

Table 1: *Description of the Monte Carlo samples used for the analysis. First column contains particle type, the second and third ones contain the generated momentum range and corresponding kinetic energy range and the last column contains a number of generated events or events satisfying the Level-1 trigger conditions (see text).*

Particle	Momentum range [GeV/c]	E_k/nucl [GeV]	Number of events
First type (acceptance indirect)			
d	0.9, 1.0, 1.1, 1.2, 1.3, 1.4, 1.5, 1.75, 2, 3, 4, 5, 6, 7, 8, 10, 16, 17	0.1-7.6	generated events $5 \cdot 10^6$ (for every energy point)
$\bar{p}$	1, 2, 5, 10	0.4-9.1	
p	1, 2, 5, 10	0.4-9.1	
Second type (acceptance direct)			
$\bar{d}$	1,2,4,8,16	0.13-7.1	generated events
$\bar{p}$	1,2,4,8,16	0.4-15	$5 \cdot 10^6$
e	1,2,4,8,16	1-16	(for every energy point)
Third type (selection optimization)			
			events accepted by LVL1
$\bar{d}$	0.5-20	0.03-9.0	$1.2 \cdot 10^6$
d	0.5-20	0.03-9.0	$1.2 \cdot 10^6$
p	0.5-10	0.13-9.1	$3 \cdot 10^6$
e	0.5-10	0.5-10.0	$7 \cdot 10^6$
$\bar{p}$	0.5-10	0.13-9.1	$3.3 \cdot 10^6$

4 Preselection

The preselection requirements are designed to identify the particles passing through the fiducial volume of the AMS-02 detector, ie. the volume filled with physics detectors and not with the additional infrastructure. The events, reconstructed in a simple way (*AMSParticle* object) must be characterized by the measurements of charge, velocity and momentum. The quality of reconstruction of these parameters is not considered at this level, because it will depend on type of analysis carried out

in the following steps. The preselected events define the "geometrical acceptance" of the detector.

The preselection requirements are similar to the ones used in previous AMS-01 analyses [2, 13], but are tailored to the AMS-02 detector.

The event reconstructed in AMS-02 contains usually just one particle passing through the detector. Therefore the basic reconstructed object in AMS analysis is called *AMSParticle*. It is reconstructed matching the measurements from the different detectors, depending on the trigger. For example in case of *AMSParticle* obtained from TOF and Tracker detectors a measurement of velocity in TOF and a reconstruction of track in Tracker is required, together with measurement of charge coming from at least one of the detectors.

The first request applied in this analysis is to have only one *AMSParticle* object reconstructed. Efficiency of this selection on antideuteron sample is 58% and the rejected events usually do not contain any *AMSParticle*. The AMS-02 acceptance and thresholds have been chosen so that usually one particle which can be measured enters the detector.

The *AMSParticle* object to be used in the following analysis, is also required to satisfy the following conditions:

- have velocity measurement in TOF (not only TOF trigger),

- have track reconstructed in Tracker (to measure momentum),

- have track reconstructed in TRD (necessary for further rejection of electron background),

- the absolute charge measured for the particle is 1 (to reject alpha particles, which are abundant in cosmic rays and which can be reconstructed with underestimated mass faking antideuterons),

An additional selection on the event is:

- no clusters in Anticoincidence Counters in order to exclude events with interactions in the detector material (this condition is also included in proposed schemes of LVL1 trigger logic).

The cumulative efficiencies of the preselection cuts with respect to the events after LVL1 trigger conditions are presented in Table 2. The difference between proton and antiproton efficiencies is due to different attenuation lengths for matter and antimatter. It is discussed in Section 5 where a corresponding factor is found to correct for this effect.

Table 2: *Cumulative efficiency of preselection with respect to LVL1 trigger for various particle samples.*

	selection efficiency				
particle type	$\bar{\text{d}}$	d	p	e	$\bar{\text{p}}$
Only one AMSParticle	0.58	0.61	0.54	0.40	0.37
+ AMSParticle has β	0.58	0.61	0.54	0.40	0.37
+ AMSParticle has track in TRK	0.40	0.41	0.37	0.28	0.26
+ AMSParticle has track in TRD	0.32	0.33	0.29	0.23	0.20
+ AMSParticle absolute charge is 1	0.32	0.33	0.29	0.22	0.20
+ no ACC Clusters in event	0.29	0.30	0.27	0.17	0.17
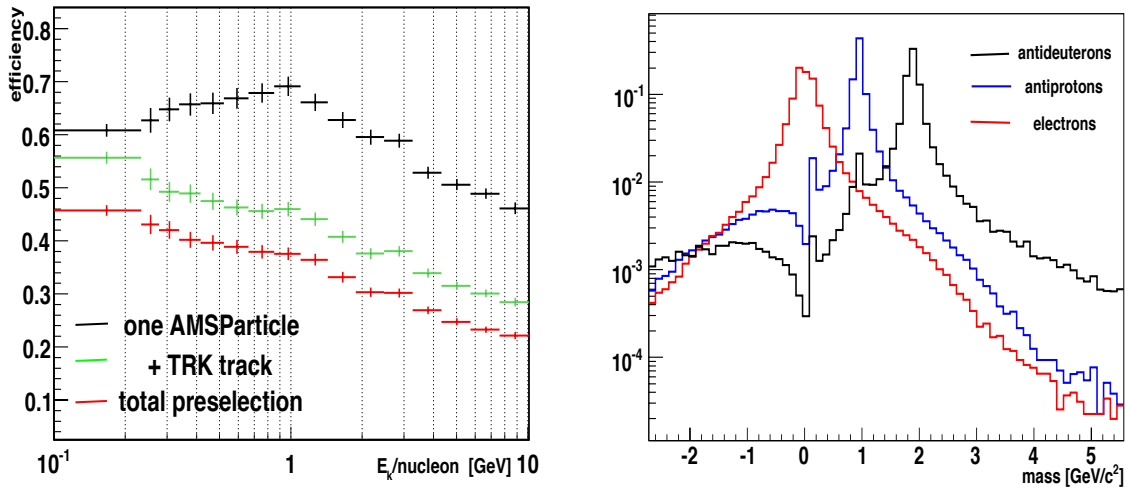
Figure 2: *Left plot: efficiency of preselection on the antideuteron sample as a function of generated kinetic energy per nucleon (*E_k/nucleon*). The average efficiency for the sample is 29%. Black points shows the efficiency of AMSParticle=1 requirement, green ones add the requirement of existence of track in Tracker and the red ones shows the final efficiency. Right plot: normalized distributions of reconstructed mass of particles passing the preselection. Negative masses correspond to particles reconstructed with $\beta > 1$.*

On the left plot of Figure 2 the preselection efficiency as a function of the generated antideuteron kinetic energy per nucleon (E_k/nucleon) is presented. Antideuterons of high energies tend to be triggered with higher efficiency, however they are not efficiently reconstructed. Already the requirement of simple reconstruction of one *AMSParticle* object (black points) is more restrictive for high-energy antideuterons, but the most critical requirement is the existence of well reconstructed

9

track in TRK (green points). The red points show the total preselection efficiency for antideuteron sample.

On the right plot of Figure 2 the distributions of reconstructed mass of antideuterons, antiprotons and electrons after preselection are presented. The distributions, normalized to 1, illustrate the amount of events in tails which must be removed by the subsequent analysis selections.

5   Acceptance

To estimate AMS-02 sensibility to antideuteron flux, the detector acceptance must be determined. In this work the acceptance has been estimated separately for deuterons, antideuterons, electrons and antiprotons.

Two approaches to estimation of antideuteron acceptance are presented. In the first approach deuterons and an antimatter correction factor are used. In the second approach a newly-generated antideuteron sample has been explored.

In the first approach to estimate antideuteron acceptance the events are generated on a surface of a box containing AMS-02 detector. Assuming that the particles are generated randomly on the surface and isotropically in angle the acceptance $A_0(E)$ as a function of energy is expressed by Equation 2.

$$A_0(E) = \int_S d\sigma \cdot \hat{r} \int_\Omega d\omega \times \frac{N_{acc}(E, \Theta, \phi)}{N_{gen}(E)} = \frac{6S}{2} \int_{2\pi} d\phi \int_0^1 \frac{N_{acc}(E, \Theta, \phi)}{N_{gen}(E)} d(cos^2\Theta) \quad (2)$$

where S is the area of the one surface of the cube (3.9×3.9 m^2), Ω is a solid angle (whole upper hemisphere), $d\sigma$ is a surface element of the detector, Θ and ϕ are the angles in polar coordinates, $N_{gen}(E)$ and $N_{acc}(E)$ are numbers of generated and accepted events for a given energy. The $cos^2\Theta$ factor in the Equation 2 suggests that the efficient particle generation could follow a $cos^2\Theta$ dependence (therefore not isotropic in Θ). The particles arriving with large Θ have low probability to be accepted and contribute less to the geometrical acceptance than the particles with small Θ (ie. downward-going ones).

Using a $cos^2\Theta$ dependence in event generation and integrating over angles Θ and ϕ the Equation 3 is derived.

$$A_0(E) = \frac{6S}{2} \int_{2\pi} \frac{N_{acc}(E, \Theta, \phi)}{M_{gen}(E, \Theta, \phi)} d\phi = 6\pi S \times \frac{N_{acc}(E)}{M_{gen}(E)} \quad (3)$$

where $M_{gen}(E) = N_{gen}(E)/cos^2\Theta$, the number of events generated at energy E in $cos^2\Theta$ bin.

The accepted events do not only trigger the experiment but are also requested to satisfy the preselection cuts (Section 4). The obtained deuteron acceptance as a function of energy is presented on the left plot of Figure 3.

The second step is the evaluation of the antimatter correction factor to deuteron acceptance. Here it is derived from proton and antiproton samples [2]. For every momentum bin p the antimatter correction factor (corr(p)) is obtained as a ratio of antiproton to proton acceptances. The correction factor is shown on the right plot of Figure 3, where it is fitted with Formula 4.

$$\text{corr(p)} = 1 - \frac{p_1}{p^{p_2}} \quad (4)$$

11
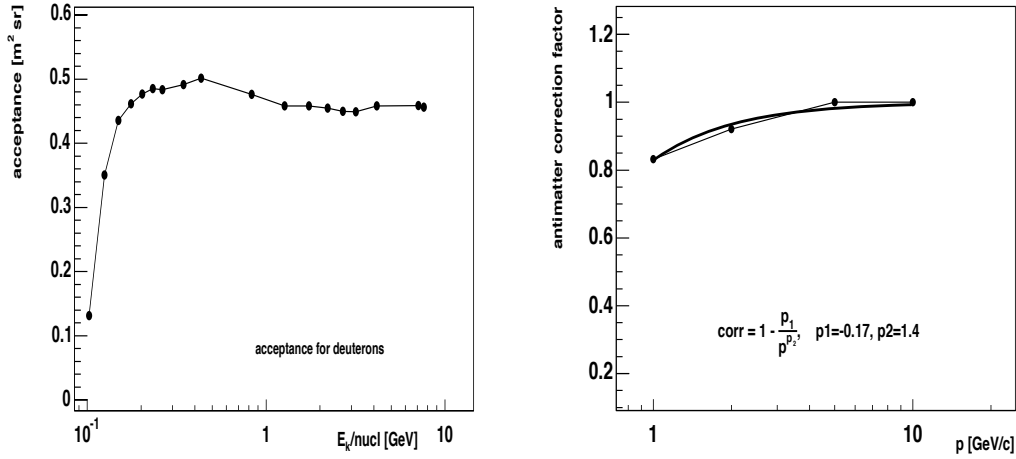
Figure 3: *Left plot: AMS-02 acceptance for deuterons. Right plot: antimatter correction factor based on comparison of acceptances for protons and antiprotons.*
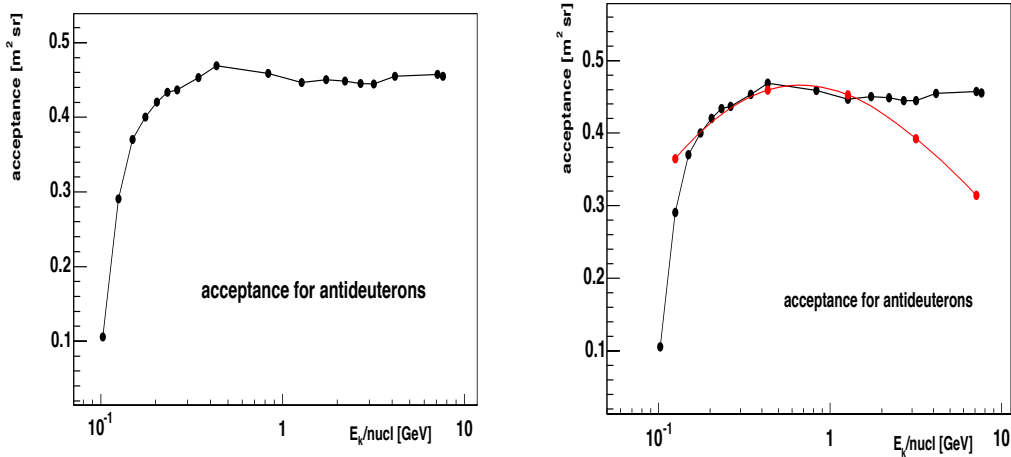
Figure 4: *Left plot: effect of use of the correction factor on acceptance from Figure 3. Right plot: comparison of antimatter-corrected deuteron acceptance (black points) with directly simulated antideuterons acceptance (red points).*

where fit parameters $p_1 = -0.17$ and $p_2 = 1.4$ Applying the correction factor to deuteron acceptance the estimation of antideuteron acceptance is obtained. It is presented on the left plot of Figure 4.

The values of antideuteron acceptance are fitted with Formula 5, which describes the energy dependence of acceptance [14].

12

$$A = p_0 \cdot exp\left(-\frac{z + exp(-z)}{2}\right) \qquad (5)$$

The variables in the Formula 5 are $z = \frac{-x - p_1}{p_2}$ and $x = \log(p)$. The values of the fit parameters are presented in Table 3. The fit with a function of the logarithm of momentum reflects the behaviour of acceptance which changes rapidly for low momentum and slowly for high momentum values. From the Figure 4 one can see that the geometrical acceptance for antideuterons reaches value of $0.4 \text{ m}^2\text{sr}$ for kinetic energy per nucleon of about 0.2 GeV and remains on the plateau for higher energies.

The above approach has been verified using the more straightforward method with a sample of antideuterons. The sample was limited to antideuterons in a few momentum bins only (1, 2, 4, 8 and 16 GeV/c) and generated on the top surface of the AMS-02 (the previous sample was generated from box around the detector). The antideuteron description in AMS-02 is preliminary and the statistics was limited.

For antideuteron sample the Formula 6 has been used to evaluate geometrical acceptance as a function of energy ($A(E)$). It is different from Formula 3 by a factor 6 because particles in this sample have been generated only on the top surface of the box.

$$A(E) = \pi S \times \frac{N_{acc}(E)}{M_{gen}(E)} \qquad (6)$$

The comparison of antideuteron acceptances based on these two approaches is presented on the right plot of Figure 4. In a large part of kinetic energy range both acceptances are comparable. In low kinetic energy region the acceptance obtained in the first mode (from deuterons) presents a strong threshold effect, which can be particularly important in Dark Matter studies. The lack of this effect in the second approach is be due to the limited available statistics of antideuteron events.

The acceptance has also been estimated for antiprotons and electrons, which are the most important backgrounds to antideuteron search. The results are presented in Table 3. The antiproton acceptance calculated this way is by about 15% smaller than the antideuteron one. The electron acceptance is smaller by about 30%.

Table 3: *Values of parameters for acceptance parametrization obtained with fitting Formula 5. $\bar{\text{d}}$ (1) stands for the first approach to antideuteron acceptance calculation while $\bar{\text{d}}$ (2) stands for the second approach.*

particle	p_0	p_1	p_2
$\bar{\text{d}}$ (1)	0.51	0.82	0.42
$\bar{\text{d}}$ (2)	0.77	0.97	1.14
$\bar{\text{p}}$	0.63	0.71	0.93
e	0.58	0.42	0.59

6 Analysis procedure

In this Section the criteria for antideuteron selection are described. These criteria are divided in three groups according to their purposes:

1. assure the quality of the velocity measurement in Time-of-Flight (TOF) and Ring Imaging Cherenkov (RICH) detectors,

2. assure the quality of the momentum measurement and rejection events with scattering in the Tracker (TRK),

3. reject electron background and events with important scattering in Transition Radiation Detector (TRD).

The first two groups are designed to select events with well-reconstructed velocity and momentum and therefore a well-reconstruct antideuteron mass. This observable is the main discriminant against the electron and antiproton backgrounds. The last group of selection criteria, based on TRD measurements, increase the rejection efficiency of electron background and rejects events with scattering in the most upstream detector. The scattering might be particularly important for low energy particles.

6.1 Velocity measurement in Time of Flight

The Time of Flight system (TOF) provides the main AMS-02 trigger and a measurement of a particle velocity (β). To assure quality of the velocity reconstruction in TOF and to reject wrongly reconstructed events as well as background events, the requirements are applied on:

- the highest number of TOF cluster which were not used in velocity reconstruction,

- the lowest number of TOF layers used in velocity reconstruction,

- the largest distance between the position of the track extrapolation from Tracker to TOF and the position measured by TOF,

- the highest velocity value.

The possibility of use of other requirements as suggested in [2], has been investigated. Their implementation does not produce a significant impact on the present analysis. As an example a selection on χ^2_{time} of the time-fit was not considered here as it does not improve β reconstruction and events with high χ^2_{time} are often rejected by other criteria.

The efficiencies of requirements described below are summarized in Table 4.

6.1.1 Number of unused TOF clusters

The measurement of velocity in TOF is based on a straight line fit to the time-position diagram. Every point on this diagram is obtained from one TOF cluster. The fit is tested for different subsets of the clusters. If including a cluster leads to nonphysical small value of β or if the χ^2_{time} of the fit becomes too large, the cluster is not included in the fit and is marked as "unused".

In [2] no unused clusters were allowed. Efficiency of this selection was 92% for AMS-01 Monte Carlo sample. The same requirement applied to AMS-02 data gives only 71% efficiency. It is too restrictive for an analysis aimed on detection of a faint signal. In addition it weakly improves the quality of β reconstruction. Therefore in this analysis an existence of one unused TOF cluster is allowed, leading to efficiency of 94% on the antideuteron sample. The distribution of number of extra TOF clusters is presented on the left plot of Figure 5.
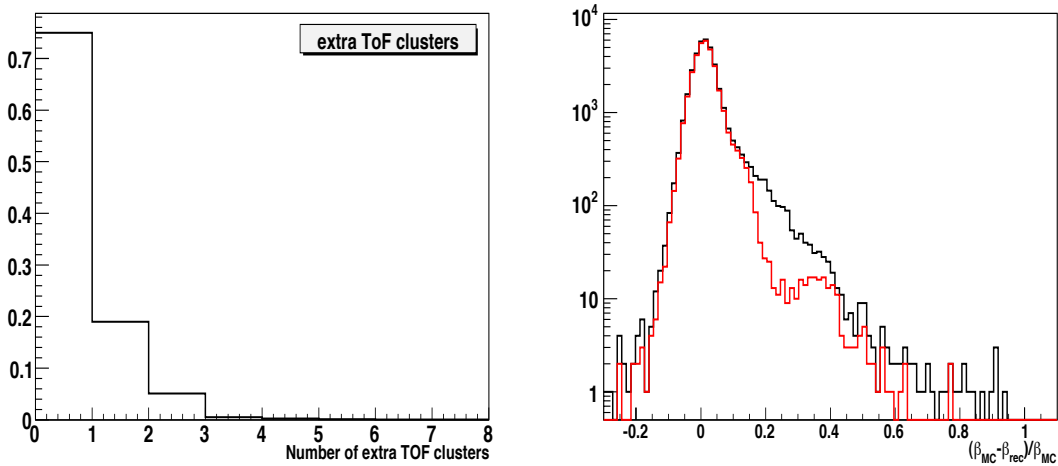
Figure 5: *Left plot: a distribution, normalized to 1, of number of unused TOF clusters. Right plot: effect of the selection on unused clusters on the quality of β reconstruction for antideuteron sample. The black line represents events after preselection, the red one represents events with the additional selection on unused TOF clusters.*

On the right plot of Figure 5 the effect of this selection on the quality of β reconstruction is presented. Almost 90% of events with reconstructed velocity underestimated by 20% to 40% are rejected by a request of having not more than one unused cluster.

6.1.2 Number of used TOF layers

At least two measurements are necessary in order to measure velocity of a particle in TOF: one from top (1,2) and one from bottom (3,4) TOF layers.

15

On the left plot of Figure 6 a distribution of a number of TOF layers used for velocity reconstruction is shown. About 5% of events in the sample have velocity reconstruction based on signal from 2 TOF layers, 22% from 3 TOF layers and the rest (about 73%) use signals from all 4 layers. Events which uses 2 or 3 TOF layers for β measurement represent a significant fraction of the sample, but rejecting them improves the quality of velocity reconstruction. On the right plot of Figure 6 the effect of the cut on quality of velocity reconstruction is presented. Black line represents events after preselection and the red represents events which pass additional requirement of use of all 4 TOF layers in velocity reconstruction. The efficiency of the additional selection is 73% with respect to preselected sample of antideuterons.
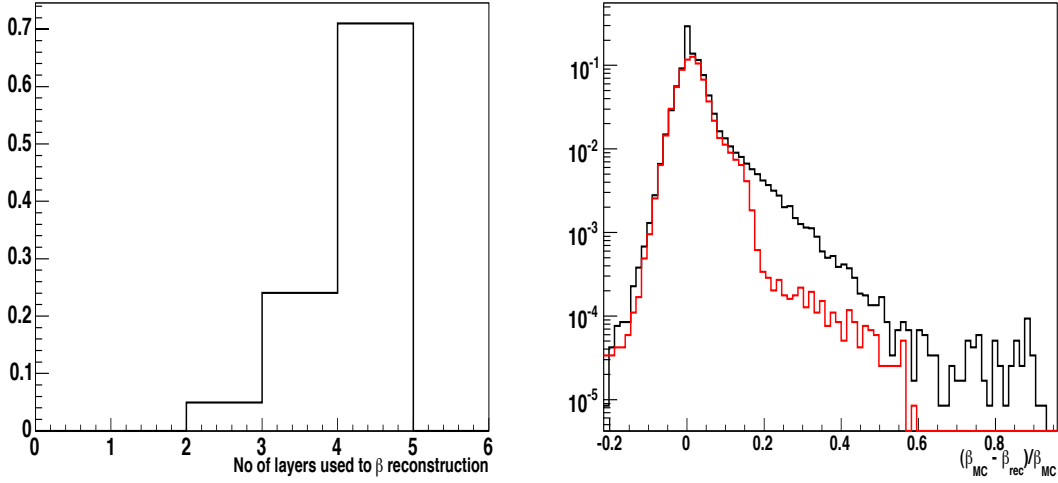
Figure 6: *Left plot: distribution of the number of TOF layers used for velocity reconstruction. Right plot: effect of the selection on the number of TOF layers ($N_{layer}^{TOF} = 4$) on the quality of β reconstruction. Black histogram is after preselection and the red one after additional selection of events with at least 3 TOF layers used for β measurement. Efficiency for antideuteron sample is 73% .*

6.1.3 Distance between cluster position and prediction from Tracker

The track measured by Silicon Tracker can be extrapolated into the TOF paddles with a great precision (see Figure 4-3 of [2]). The hit position in TOF paddle is determined from the difference in time measurements between the photomultipliers at the ends of the paddle. The TOF measurement is compared with the extrapolation from Tracker. The difference between both positions is presented on Figure 7. Every plot shows the distance between Tracker extrapolation and TOF measurements in

16

the TOF paddle direction. A gaussian fit to the distributions of $|x_{TOF} - x_{TRK}|$ and $|y_{TOF} - y_{TRK}|$ is performed and the obtained σ values are in the range from 1.99 to 2.39 cm. In the following analysis only events with a distance between track extrapolation and TOF measurement lower than 2.5σ are considered.
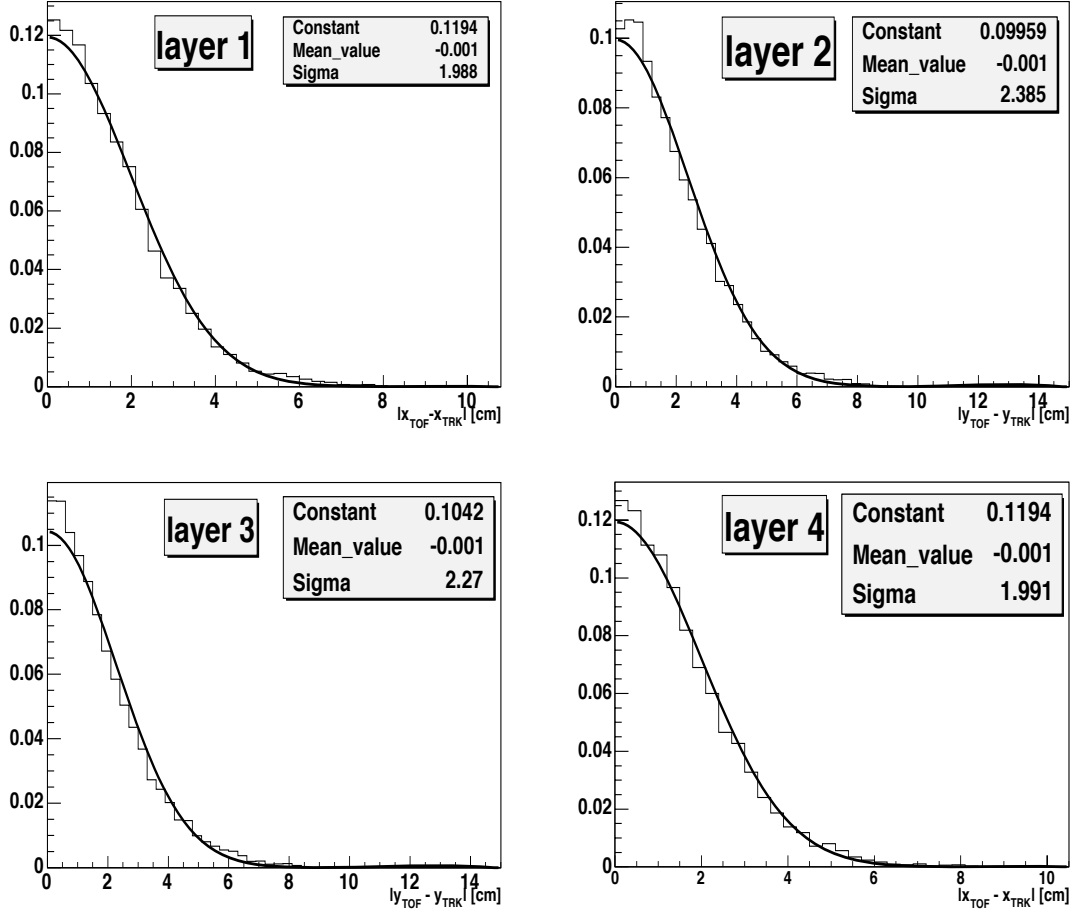
Figure 7: *Distances between TOF cluster position (x_{TOF}, y_{TOF}) and extrapolation of the track from Tracker (x_{TRK}, y_{TRK}). A gaussian fit was performed and the width σ is used to determine the value of the cut in each layer.*

The impact of this selection on quality of β reconstruction is small for antideuteron sample. The efficiency of Tracker-TOF position matching is 93% for antideuteron sample and 87% for electron sample.

6.1.4 Measured value of velocity

The limited resolution of time measurement of TOF [15] implies a resolution of the β measurement of the order of $\delta\beta = 0.04$ for high values of β. In case of particles

17

passing through AMS-02 with large incident angle the β resolution can be further deteriorated.

The mass reconstruction is very sensitive to β for fast particles (see Formula 1). To avoid the events with large error of reconstructed mass, a limit on the highest value of measured particle velocity is applied.

This limit plays a crucial role in rejecting antiproton background because antiprotons with the same momentum as antideuterons have higher β. The same is true for electron background. The distribution of measured β for antideuteron sample (after preselection) is presented on the left plot of Figure 8. On the right from vertical red line unphysical values are presented ($\beta > 1$).

A careful study is performed in order to choose a value which gives the highest significance on the antideuteron flux. This choice depends on the flux of antideuterons, which is unknown (see discussion in Section 7). In the Figure 9 the efficiencies with respect to preselected sample as a function of the cut value, for antideuteron, antiproton and electron samples are shown. The left plot presents the cut in the whole reconstructed mass range and the right one for masses above 1.6 GeV/c^2. Results presented here are for cut value $\beta_{\mathrm{TOF}} < 0.86$, but it should be tuned in range $0.82 - 0.88$.
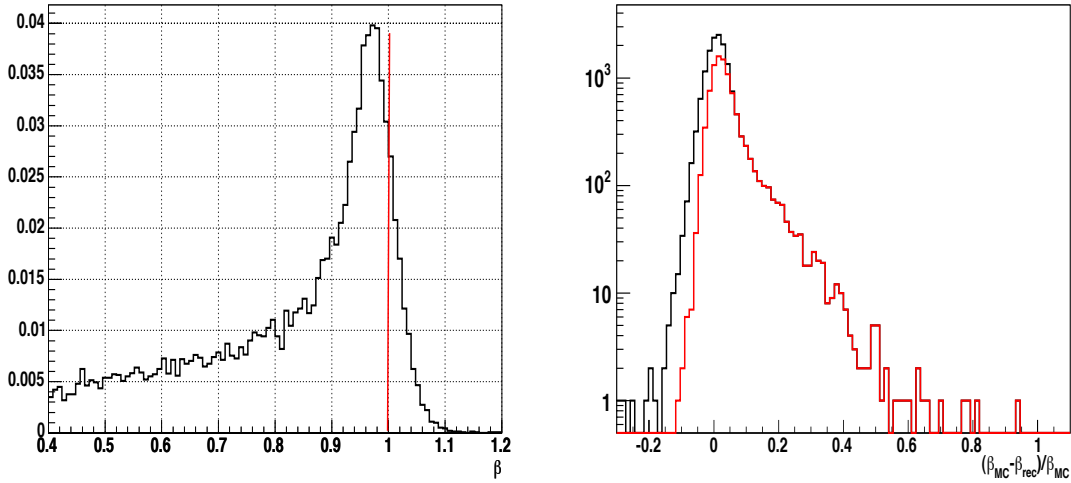
Figure 8: *Left plot presents the distribution of the β reconstructed in TOF for antideuteron sample. The right plot presents result of the $\beta_{\mathrm{rec}} < 0.86$ selection on the quality of β reconstruction. The black histogram represents events after preselection and the red one after additional selection on $\beta_{\mathrm{rec}} < 0.86$. The selection affects mainly events with overestimated velocity ($\beta_{\mathrm{rec}} > \beta_{\mathrm{MC}}$).*

On the right plot of Figure 8 the effect of this selection on the quality of the reconstructed β is shown. The black histogram presents the quality of β reconstruction af-

18

ter preselection and the red one adds the selection on maximal value of β measurement in TOF. The selection affects mainly events with overestimated β . Its efficiency for antideuteron sample is 45% with respect to events after preselection.
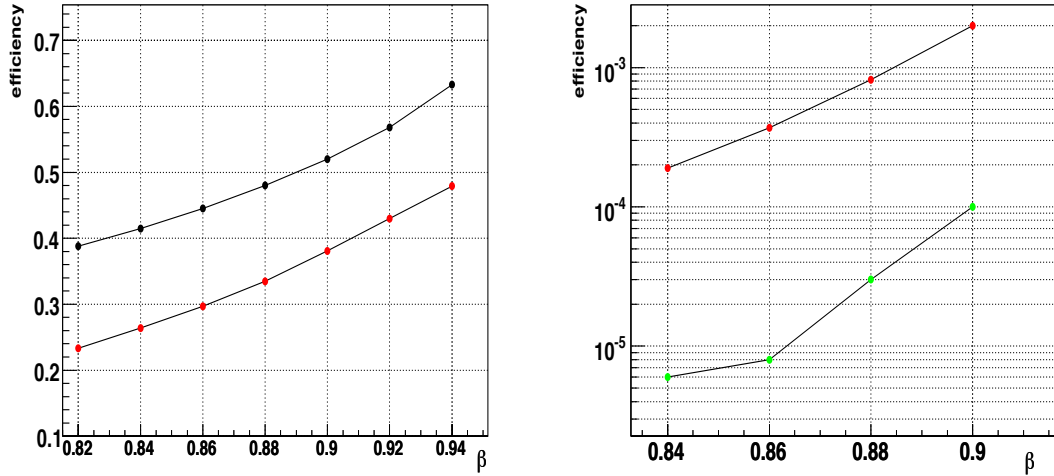
Figure 9: *Left plot: the efficiency of the selection on the highest value of velocity. Black dots are for antideuteron sample and the red ones for antiprotons. Right plot: efficiency in mass window for antiprotons (red dots) and electrons (green dots).*

A small fraction of events (0.1%) present in the sample have negative β . These events correspond to upward-going particles, but the particles in the sample are always generated in the downward direction, therefore the events with negative β are due to errors of measurements in TOF. These events are rejected.

6.2   Velocity measurement in Ring Imaging Cherenkov

The selection applied to the β measurement in Ring Imaging CHerenkov detector (RICH) is based on suggestions [16, 17]. For the events having a reconstructed ring in RICH, associated with *AMSParticle* a selection presented in this Section is applied. If the event is selected the RICH velocity measurement is used in the mass reconstruction, otherwise the TOF branch of analysis is tested.

The particles passing through RICH produce Cerenkov light if their kinetic energy is higher than 2.5 GeV/nucleon, which is a threshold characteristic to aerogel radiator. The threshold of NaF radiator is lower (0.5 GeV/nucleon) but its acceptance is only around 10% of the total RICH acceptance. The threshold effect implies that only 18.5% of events from Monte Carlo sample produce a ring in RICH.

It should be stressed that the following analysis of RICH events is preliminary and the detailed study will be presented in [18]. This analysis is focused on low energies, where Dark Matter signal could be visible in antideuteron spectrum, therefore the TOF selection were studied in details.

6.2.1 Single particle crossing photomultiplier plane

The particle which produces the ring in RICH detector usually, when crossing the plane with photomultipliers, leaves a high signal in at least one of them. In order to assure that this signal does not deceive the ring-finding algorithm, the requirement of existence of not more than one reconstructed AMSParticle object which crosses the PMT plane is imposed.

Efficiency of this selection on the antideuteron sample is almost 18.5% with respect to events after preselection and almost 100% with respect to events with a RICH ring.

6.2.2 Particle not hitting the ring

Events presenting a particle hit in photomultiplier plane close to the reconstructed Cerenkov ring are excluded because the amount of photoelectrons generated by the particle hit overcomes the Cerenkov signal, and therefore spoils the RICH measurement.

Efficiency of this criteria for the antideuteron sample is 18.3% with respect to events after preselection and almost 100% with respect to events with a RICH ring.

6.2.3 Number of collected photons consistent with Z=1 particle

The intensity of Cherenkov radiation, proportional to the number of photoelectrons produced in photomultipliers, depends of the absolute value of the charge of particle. This intensity is predicted by Monte Carlo simulation for particle with $|Z| = 1$ and compared with the measured number of photoelectrons.

It is assumed here that if the ratio of the two numbers is smaller than 2 (see left plot of Figure 10) than the number of registered photoelectrons is compatible with $|Z| = 1$ hypothesis.

On the right plot of Figure 10 the improvement of the quality of velocity reconstruction in RICH due to discussed selection is presented. A reduction of the tails of poorly reconstructed events is visible. Efficiency of the selection for antideuteron sample is 16.1% with respect to preselected events and 87% with respect to events with a RICH ring.

6.2.4 Quality of reconstructed ring

The quality of the reconstructed ring is measured by a likelihood probability. The distribution of this probability is shown on the left plot of Figure 11. The value of the cut suggested by [16] is 0.03.

Efficiency of this selection for antideuteron sample is 17.2% with respect to preselected events and 93% with respect to events containing a ring. The effect of the cut on the accuracy of β reconstruction is shown on the right plot of Figure 11 The
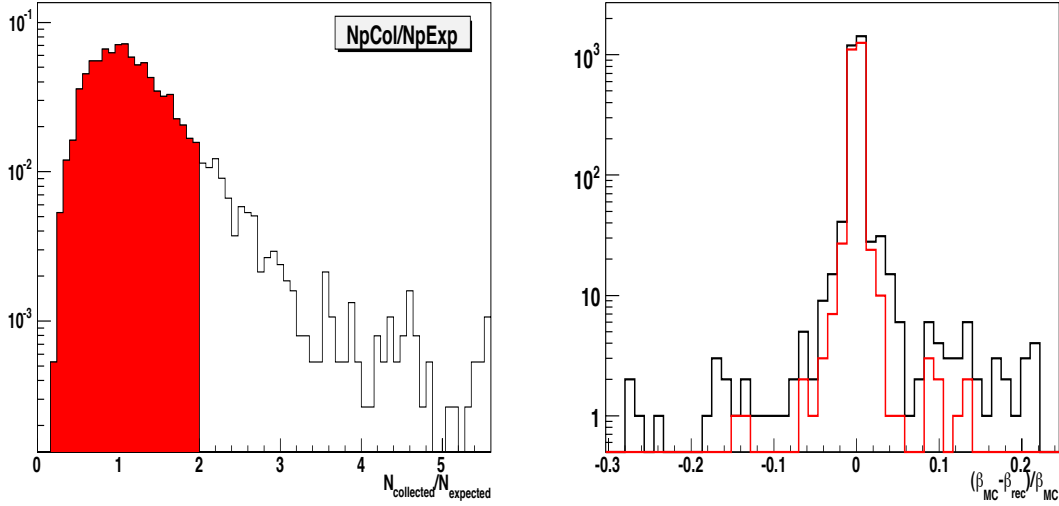
Figure 10: *Left plot: number of collected divided by number of expected photoelectrons - distribution for antideuterons with selection represented by the red area. Right plot: effect of the proposed selection on the quality of velocity reconstruction in RICH. Black histogram refers to preselected events with a reconstructed ring, the red histogram adds the selection discussed in Section 6.2.3.*

black line is for events passing preselection cuts and the red one is after additional cut on quality of the RICH ring.

6.2.5 Number of unused RICH hits

A ring is reconstructed from at least 3 hits in RICH. More than one ring can be reconstructed for each event, but only one is associated to the *AMSParticle*. Therefore a number of hits remain not associated to the *AMSParticle*. They are called "unused hits".

Events with more than 5 unused hits are rejected. The efficiency of this selection is 12.1% with respect to preselected antideuteron events and 65.4% with respect to events with a RICH ring.

6.2.6 Upper limit on β and compatibility with TOF

For the reasons similar to the ones presented in case of TOF measurement (Section 6.1.4) a selection on the value of measured β is performed.

The error of β measurement in RICH is about 0.5%, what suggests that the highest acceptable value of β measured in RICH is $\beta_{\text{RICH}} = 0.99$ corresponding to cut on antideuteron momentum of 13 GeV/c and kinetic energy about 5.5 GeV/nucleon.

21
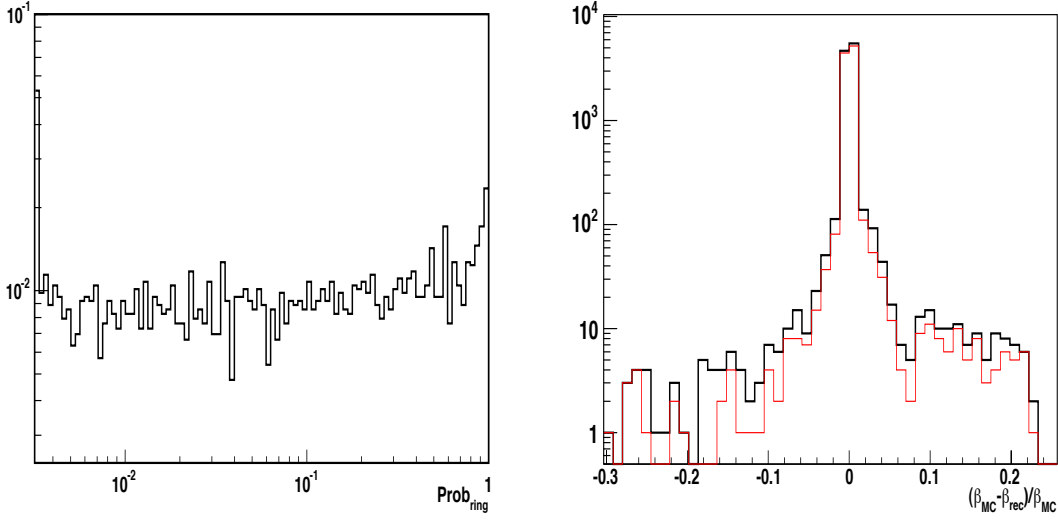
Figure 11: *Left plot: distribution of likelihood probability of ring. The proposed value of the cut is 0.03. On the right plot the effect of the selection on the quality of β reconstruction is shown. Black line is for events after preselection and the red one adds the selection on quality of the ring.*

The efficiency of this selection on antideuteron sample is 11.4% with respect to preselected events and 62% with respect to events with RICH ring.

In addition a RICH-TOF measurement compatibility is requested to be at the level of 10%:

$$0.9 < \frac{\beta_{\text{TOF}}}{\beta_{\text{RICH}}} < 1.1 \tag{7}$$

A small part of events with underestimated and overestimated β are removed by this selection. The efficiency for antideuteron sample is 18.1% with respect to preselected events and almost 98% with respect to events with a RICH ring.

6.2.7 Energy deposition in lower TOF layers

This selection is aimed to rejection particles which are subject of important scattering just before entering the RICH.

The selection is based on unused TOF clusters (see Section 6.1.1). The event is rejected if there are unused clusters in layers 3 or 4 or if the energy deposited in clusters in layers 3 and 4 is higher than 4 MeV per layer.

Efficiency of this selection in antideuteron sample is respectively 87.5% and 81.9% with respect to preselected events. Efficiencies with respect to events containing a RICH ring are respectively 86% and 95%.

6.3 Momentum reconstruction

Silicon tracker provides two very important measurements for this analysis: a rigidity and a sign of charge. The quality of measurement of rigidity is important for particle mass determination therefore it is crucial for rejection of antiproton and electron backgrounds. The charge confusion for momenta below 10 GeV is negligible - about 10^{-8}. Therefore the backgrounds from particles with wrongly reconstructed sign of charge, mainly protons and deuterons, are efficiently reduced.

The requests on the momentum reconstruction of the track are designed for:

- reject events with wrongly reconstructed momentum ie. $|\frac{\mathrm{p_{gen}-p_{rec}}}{\mathrm{p_{gen}}}| >> 0$ ([3]),

- assure a good reconstruction of the sign of charge obtained from track curvature,

- reject events with complicated topology in the Tracker (ie. events which present difficulties for reconstruction algorithm),

- reject events with poor quality of track fit (χ^2),

- reject background events (for instance the selection on number of hits in the Tracker rejects more electrons than antideuterons).

These goals are achieved by performing selection on measurements from Tracker. However further selections performed on upstream detectors, presented in Section 6.4, also improve momentum reconstruction by removing of the events with important interactions in the upstream material.

The selection on the track in the Tracker is based on the following observables:

- number of hits used for track reconstruction,

- χ^2 of the track fit,

- compatibility of the rigidity measured with use of different track algorithms,

- value of measured momentum,

- energy in tunnel (core) around the track.

Some of the selections used in previous analyzes are not present here. For example the criteria based on comparison of the momentum measured in the two halves of Tracker turns out to be ineffective for low momenta [19].

In the following the chosen selection is discussed in details.

---

[3]We remind that for real data $p_{gen} = p_{real}$

6.3.1 Number of hits used for track reconstruction

In order to assure high precision of momentum measurement, the track reconstruction is based on at least 5 hits on different silicon planes. The heavy particles, as deuterons, have higher probability to leave a hit than light particles like electrons.

On the left plot of Figure 12 the number of hits per track is presented for antideuteron (black line) and electron (red line) samples. Rejecting events with only the minimal number of hits per track reduced the antideuteron signal by 7% while electron background is reduced by 21%. The quality of momentum reconstruction is slightly improved.
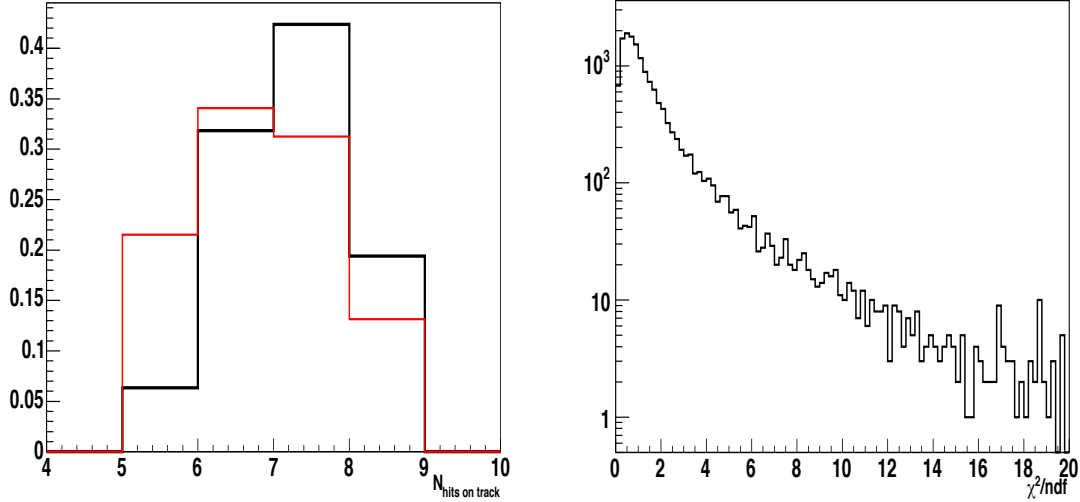
Figure 12: *Left plot: distribution of number of hits per track in Tracker for antideuterons (black line) and for electrons (red line). Right plot: quality of track fit expressed in χ^2 per degree of freedom of the fit (see Section 6.3.2).*

6.3.2 Track fit quality

Three algorithms are used by a current track reconstruction software: Path Integral method [20], GEANE fit [21] and Fast Fit method [22].

Path Integral is designed for high momentum particles so it is not used for this analysis. GEANE fit is adopted from CERN libraries. The Fast Fit method has better overall efficiency than GEANE fit, therefore it is used as a basic track-finding algorithm.

On the right plot of Figure 12 the χ^2/ndf (ndf is the number of degrees of freedom of the fit) distribution is presented for the antideuteron sample. To identify a selection criteria based on this variable, the efficiency on antideuteron sample ϵ is plotted

24

as a function of χ^2/ndf on the left plot of Figure 13. This curve is characterized by two changes of slope for χ^2/ndf value about 2 and about 3. This change of slope is not correlated to the number of hits on the track.

Following this consideration a discriminant value equal to 3 has been imposed corresponding to an efficiency of 81.5% with respect to preselected events on antideuteron sample.
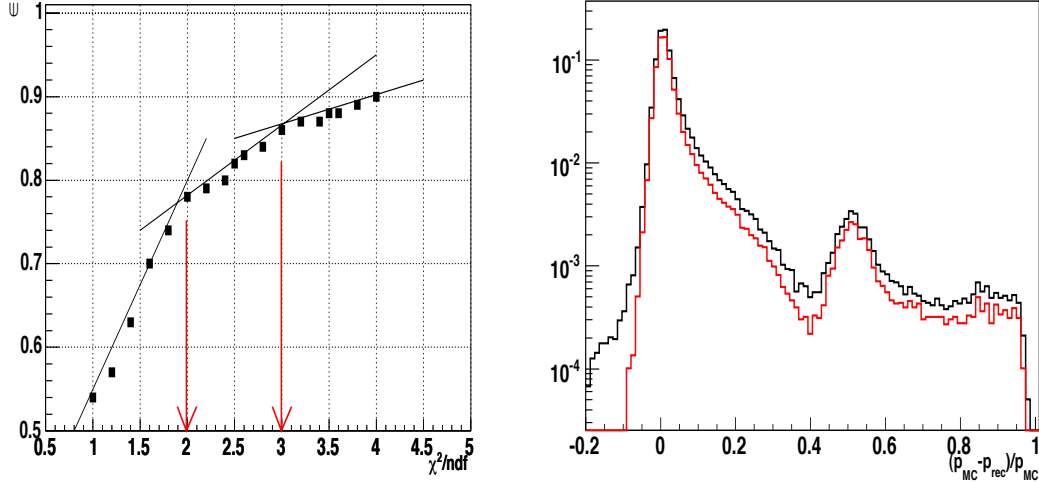
Figure 13: *Left plot: efficiency (ϵ) of the selection on χ^2/ndf as a function of the cut value. Right plot: quality of momentum reconstruction for antideuteron sample after preselection (black line) and after selection on the number of hits on track and on χ^2 (see Section 6.3.2).*

This selection has a high efficiency in removing events with overestimated momentum but very limited on events with underestimated momentum. The distribution on the right plot of Figure 13 presents the quality of momentum reconstruction. The tail of the distribution has two characteristic components. The first with values of $\frac{p_{MC} - p_{rec}}{p_{MC}}$ below 0.4 (ie. reconstructed momentum is smaller than generated by 10% to 40%) and the second one with $\frac{p_{MC} - p_{rec}}{p_{MC}} > 0.4$ and with a peak at value 0.5. This peak corresponds to events where antideuteron interacts strongly and dissociates into antiproton.

The first component of the tail is caused mainly by low momentum antideuterons loosing a part of their initial energy in multiple scattering in the TRD. These events will be discussed in Section 6.4, where a selection based on TRD is proposed.

6.3.3   Compatibility of different tracking algorithms

As explained in the previous Section there are different tracking algorithms, which give different values of reconstructed rigidity. To determine mass with small error a

very precise measurement of momentum is needed. The precision of velocity measurement in TOF is of the order of 4%. To keep mass error determined by the velocity measurement even for low energy particles the request to have error on momentum below error on velocity is imposed (see Equation 1, consider $\gamma = 1.1$ for antideuterons with kinetic energy of 0.1 GeV/nucleon - the contribution of momentum error to mass error is similar to the contribution of velocity error). To reach this precision an error of the method of momentum determination should be smaller than $\frac{\delta\beta}{\beta}$. Therefore a compatibility between rigidity calculated by Fast Fit method ($R_{FastFit}$) and the one calculated by GEANE algorithm (R_{GEANE}) is required to be better than 3%, ie.:

$$0.97 < \frac{\mathrm{R_{GEANE}}}{\mathrm{R_{FastFit}}} < 1.03 \tag{8}$$

On the left plot of Figure 14 the distribution of $\frac{\mathrm{R_{GEANE}}}{\mathrm{R_{FastFit}}}$ for different particle types is presented. On the right plot the impact of the compatibility requirement (Equation 8) on the quality of momentum reconstruction is shown. This selection removes effectively events with overestimated momentum and also a fraction of events with momentum underestimated by 10-40%.
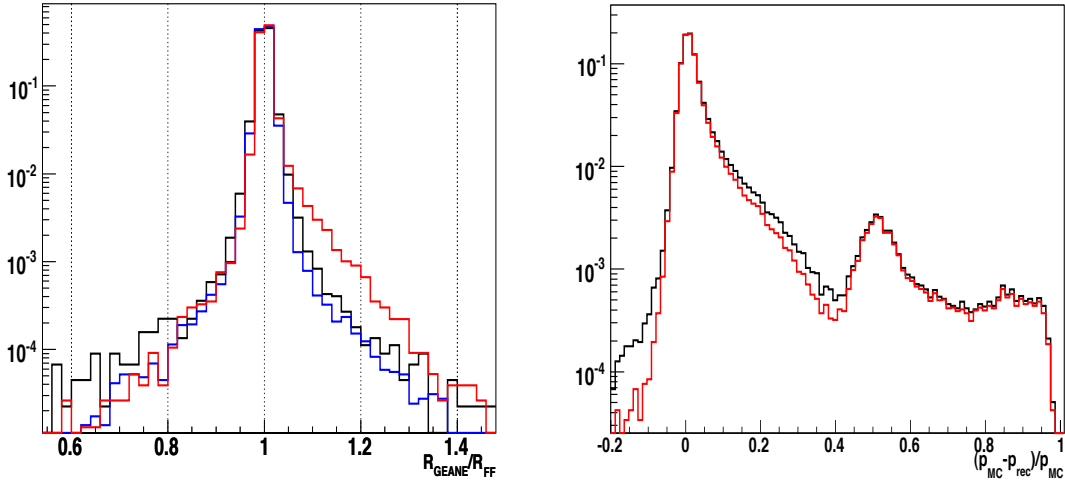
Figure 14: *Left plot: distribution of* $\frac{\mathrm{R_{GEANE}}}{\mathrm{R_{FastFit}}}$ *for antideuterons (black line), antiprotons (blue line) and electrons (red line). Right plot: the effect of the rigidity compatibility requirement on the quality of momentum reconstruction for antideuterons.*

6.3.4   Reconstructed momentum threshold

A further discrimination is applied with use of the threshold of measured momentum. The threshold for momentum measurement is a simple consequence of the value of

the AMS-02 magnetic field: particles with momentum below threshold bend in the tracker magnetic field and never reach the down TOF to trigger the data acquisition.

The Monte Carlo samples are generated with minimal momentum 0.5 GeV/c, but the momentum threshold for antideuterons corresponds to about 0.85 GeV/c. Below that value the Level 1 trigger efficiency (which includes the track reconstruction efficiency) falls down below 1%. Events with momentum below threshold are rejected, because this value of measured momentum can only be a result of misreconstruction.

The effect of this selection on $\frac{p_{MC} - p_{rec}}{p_{MC}}$ distribution for antideuterons and antiprotons is shown on the Figure 15 (green line). This selection efficiently removes events with momentum underestimated by 10-40%. The efficiency on deuteron sample with respect to events after preselection is 95.5%.
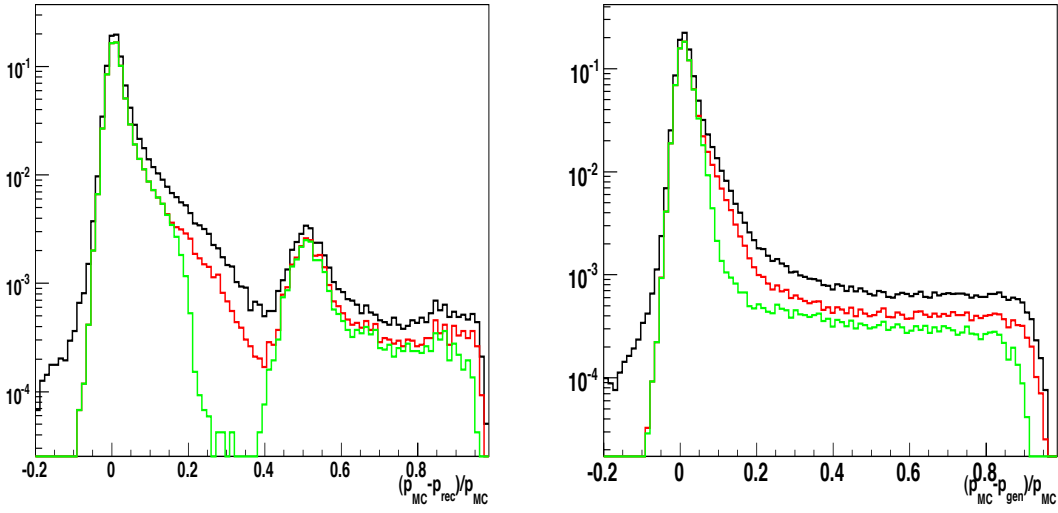
Figure 15: *Distribution of $(p_{MC} - p_{rec})/p_{MC}$ after preselection (black histogram) and after selections on number of hits on track, on χ^2 of the track fit and GEANE-FastFit compatibility (red line) and, in addition, on minimal momentum (green line). Left plot is for the antideuteron sample and the right for the antiproton one.*

6.3.5 Energy deposited in track proximity

To exclude events with significant amount of scattering inside the Tracker, a selection has been designed based on energy deposited on the track and in the track proximity. In this selection not only energy of the clusters used to track fit are taken into account, but also unused nearby hits.
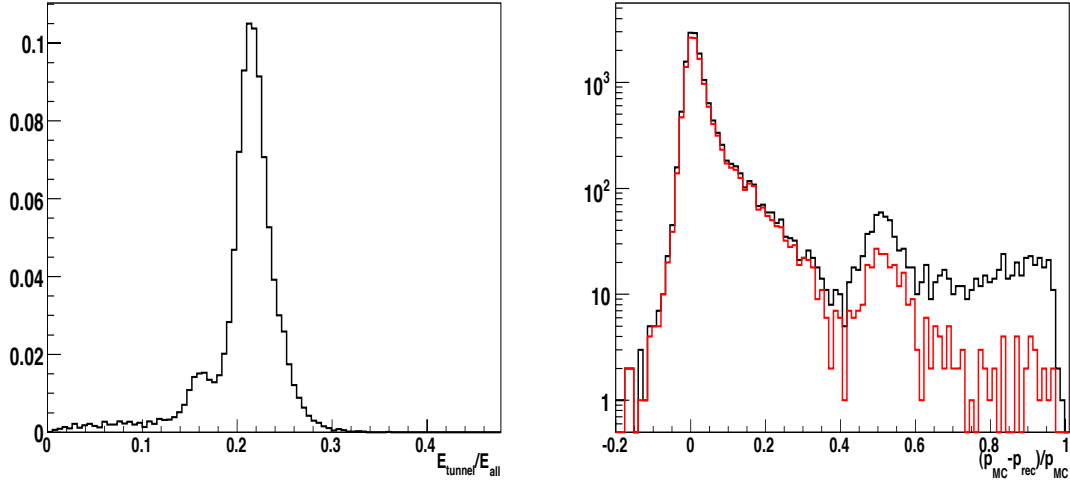
Figure 16: *Left plot: ratio of energy deposited on the track to the total energy of all hits in Tracker (E_{all}). Due to hit ambiguity the distribution is not approaching one. Right plot: effect of requirement $E_{track}/E_{all} > 0.175$ on quality of momentum reconstruction. The events after preselection are marked with black line and events after additional selection on energy deposited in track proximity with red line.*

The distances between the track position and the hit position in every layer are shown on Figure 17. This distances are small for internal layers (2-6) and increase for external layers (1 and 7-8).

For every layer a gaussian fit has been performed in order to determine the width of the distribution of the distance. The first bin of the histogram is excluded from the fit, and the mean value of the fit is constrained to be 0. For the layers 7 and 8, which show large spread of the distance between track and hits, a sum of gaussian and exponential has been fitted.

The value of the maximal distance between the track and a hit was chosen to be 2.5σ. The ratio of energy deposited in the track proximity (inside a cylinder of 2.5σ radius) to the total energy of all hits is presented on the left plot of Figure 16. The distribution is not peaked close to 1 due to the hit reconstruction ambiguity (every hit measurement is repeated a few times in the Tracker ladders).

The event is accepted if most of the energy in Tracker is deposited in the track proximity, ie. $E_{track}/E_{all} > 0.175$. Efficiency of this selection on the antideuteron sample is 86.4%. The improvement in quality of momentum reconstruction due to the selection is presented on right plot of Figure 16. This selection has a strong effect (larger than 50%) in the reduction of events with underestimated momentum.
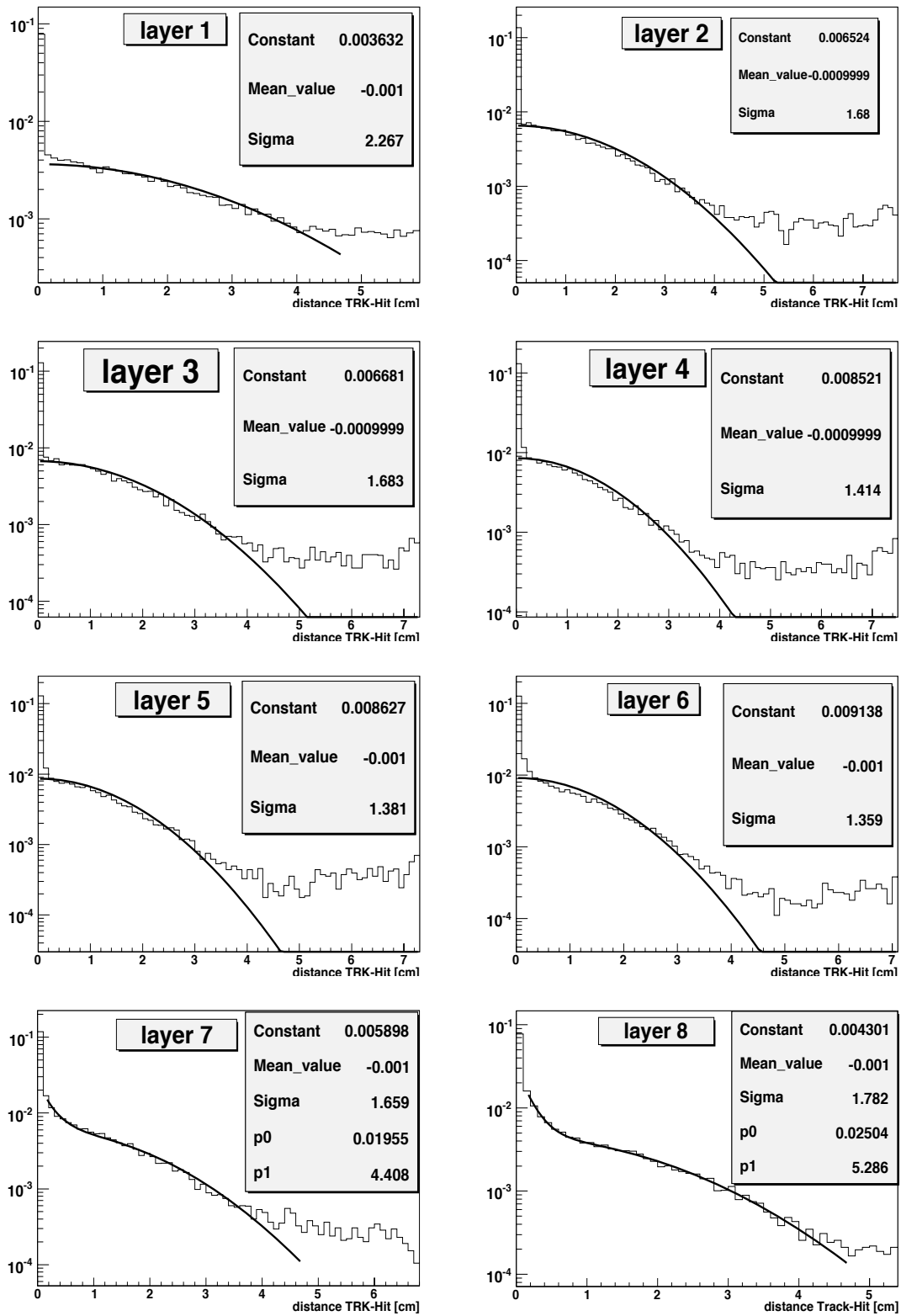
Figure 17: *Distance between track position and hit position in the Tracker layers (1-8). The lines represent gaussian fits. The layer 7 and 8 are fitted with a convolution of gaussian and exponential.*

29

6.4 Selection based on Transition Radiation Detector

The main purpose of the TRD detector is to distinguish light particles from heavy ones using the transition radiation emitted by charged particles when crossing an interface of media with different dielectric constants. In this analysis the TRD is used to reject electrons, which emit more radiation than hadrons.

The TRD constitutes a significant amount of material (about 0.11 X_0) on a particle path before it enters into the Tracker. Interactions with this material can be strong enough to change significantly the momentum and velocity of the particle. Thus, the TRD could be used to reject particles loosing large fraction of their kinetic energy in interactions before reaching Tracker.

6.4.1 Truncated mean of deposited energy

For electron/hadron separation we use the truncated mean of deposited energy [4]. On the left plot of Figure 18 the truncated average energy along the TRD track is presented for antideuterons (black line) and electrons (red line). On the right plot of the same is plotted as a function of particle momentum.
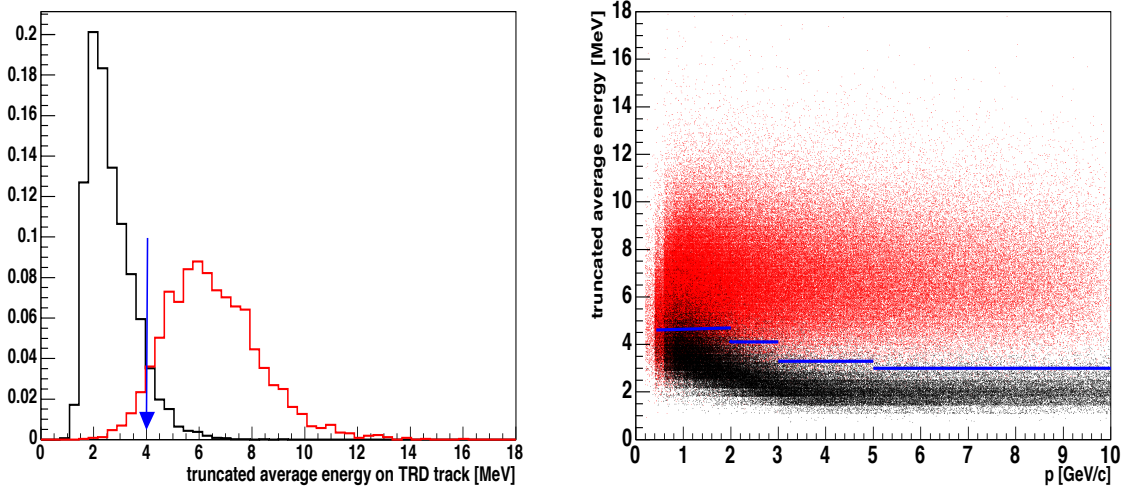
Figure 18: *Antideuteron sample (black) and electron one (red). Left plot: truncated average energy [3] deposit on the TRD track. Right plot: the same as a function of particle reconstructed momentum.*

The right plot of Figure 18 suggest to optimize the selection on truncated average energy deposited in TRD as a function of particle momentum. Four momentum

---

[4]Truncated mean energy is an average energy of TRD with the lowest and the highest values discarded.

ranges have been chosen and corresponding truncated mean energy thresholds have been assigned:

1. for p < 2 GeV/c threshold is E_{th} = 4.7 MeV,

2. for p > 2 GeV/c and p < 3 GeV/c threshold is E_{th} = 4.1 MeV,

3. for p > 3 GeV/c and p < 5 GeV/c threshold is E_{th} = 3.3 MeV,

4. for p > 5 GeV/c threshold E_{th} = 3.0 MeV

These threshold values reduce electron sample to 3.5% keeping the high efficiency of 86% for antideuteron sample. The likelihood method gives slightly lower efficiency for electrons (of the order of 2%) and a similar for antideuterons.

6.4.2 Energy fraction on TRD track

To remove events with interactions in TRD a further criteria based on the track reconstruction has been introduced. On the left plot of Figure 19 a ratio of energy deposited on the TRD track (E_{track}^{TRD}) to the total energy deposited in the TRD (E_{total}^{TRD}) is plotted. Events having an energy deposition non associated with track larger than 15% (vertical blue line) are removed from the following analysis.

On the right plot of Figure 19 the effect of the selection on the quality of momentum reconstruction is presented. The events with momentum underestimated by more than 40% are strongly supressed. The effect on the quality of the velocity reconstruction is negligible.

6.4.3 Distance between TRD track and TRK track

A further selection is applied on a distance between TRD track and extrapolation of TRK track measured on the upper surface of TRD. This distance is plotted as a function of reconstructed momentum of the particle on the left plot of Figure 20. The conclusion from this plot is that for low momentum particles this distance tends to be larger. This is due to the fact that low momentum particles tend to loose larger fraction of their energy scattering in TRD.

By removing events with particularly large distance between TRD track and extrapolation of Tracker track, events undergoing interactions with large relative energy losses are excluded. The discriminating value of the distance between TRD track and Tracker-extrapolation is a function of momentum and is indicated by a blue line on the left plot of Figure 20. The effect of this selection on quality of momentum reconstruction is plotted on right plot of Figure 20. It improves rejection of events with underestimated momentum.

31
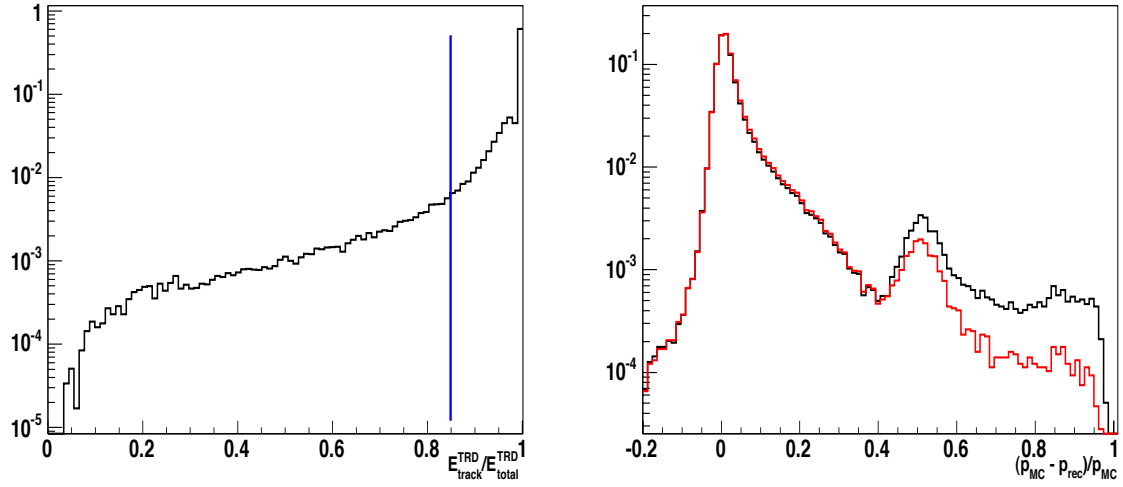
Figure 19: *Left plot: ratio of energy deposited on the TRD track (E_{track}^{TRD}) and the total energy deposited in TRD (E_{total}^{TRD}). The vertical line represents the cut value. Right plot: influence of the ($\frac{E_{track}^{TRD}}{E_{total}^{TRD}}$) selection on the quality of momentum reconstruction. A significant amount of events with misreconstructed momentum are rejected.*
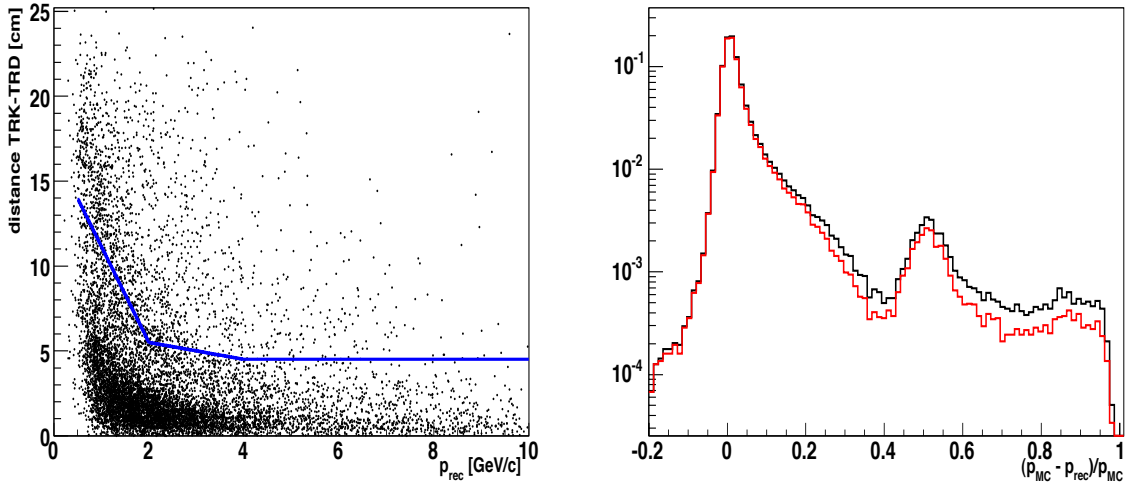
Figure 20: *Left plot: distance between TRD track and extrapolation of TRK track measured on the surface of the TRD. The blue line represents the imposed selection. Right plot: the effect of the selection on the quality of momentum reconstruction.*

7 Results

In this Chapter the efficiencies of the selection for signal and the backgrounds are summarized. The total efficiency of the selection algorithm is discussed and the resulting AMS-02 acceptance for antideuterons is calculated. The quality of the momentum, velocity and mass reconstruction is shown. Finally, the sensitivity of the AMS-02 to antideuteron flux is estimated, and the region of the supersymmetric parameter space which can be tested using the antideuteron signal is reported.

7.1 Summary of efficiencies for signal and backgrounds

The efficiencies of all the selections used in the analysis are presented in Table 4. They are calculated with respect to the preselected sample. In case of selections 2.7a and 2.7b this way of calculation of efficiency can be misleading because these selections depend on existence of RICH ring, while the selections are performed on TOF measurements.

The requirements are divided into four types, following the analysis sections: reconstruction of velocity in TOF (1), in RICH (2), reconstruction of momentum in Tracker (3) and background rejection in TRD (4). The efficiency of selection on β in TOF (1) is obtained applying the requirements from 1.1 to 1.4, but the final efficiency is not exactly equal to the product of partial efficiencies as the requirements are not independent. The total efficiency on β reconstruction (5) is, in the first approximation, equal to sum of efficiencies in TOF and RICH branches (1+2), as both groups of selection apply to different parts of the sample (with low or high kinetic energy). The mass window requirement (7) is calculated with respect to the events after the whole selection chain (6) as the mass resolution is a critical parameter for background rejection and it depends on the preceding selection. The only exception is the electron sample for which the mass window cut was tested on the sample after preselection due to lack of statistics after selection.

The efficiencies in Table 4 are the overall efficiencies for the Monte Carlo samples. The spectrum used in the Monte Carlo simulation often differs substantially from the cosmic one, therefore, for the most important particles (antideuterons, electrons and antiprotons), the energy-dependent analysis is presented. It is particularly relevant for the velocity reconstruction which is made in two detectors with different performances and sensitive in different energy ranges. Therefore the content of the Table 4, which refer to the total sample, has to be used keeping in mind this bias.

The final selection efficiency for **antideuteron** sample is about 20%. The antideuteron velocity is reconstructed with larger relative error than its momentum, therefore the cuts on the quality of velocity reconstruction determine the overall efficiency.

The selection efficiency calculated with respect to preselected events, as a function of momentum, is presented on the left plot of Figure 21. The maximal efficiency of about 40% is obtained for kinetic energy below 1 GeV/nucleon, therefore the analysis

Table 4: *Summary of the efficiencies of analysis selections. The efficiencies are calculated with respect to events passing the preselection. The cut on mass window is normalized to mass distribution after all cuts (not only preselected events). The cut number (Nr) corresponds to Section where the given cut is discussed.*

selection efficiency		particle type				
Nr	description	$\bar{\text{d}}$	d	$\bar{\text{p}}$	e^-	p
		β in TOF branch				
1.1	Extra TOF clusters < 2	0.941	0.940	0.943	0.914	0.965
1.2	at least 4 TOF layers	0.73	0.724	0.727	0.655	0.737
1.3	TOF-TRK track dist	0.931	0.920	0.912	0.878	0.919
1.4	$\beta_{TOF} < 0.86$	0.445	0.454	0.296	$5 \cdot 10^{-5}$	0.348
1	β_{TOF} reconstruction (1.1 & 1.2 & 1.3 & 1.4)	0.295	0.300	0.202	$1 \cdot 10^{-5}$	0.323
		β in RICH branch				
2.0	RICH ring exists	0.185	0.184	0.256	0.643	0.213
2.1	single particle in PMTs	0.185	0.181	0.256	0.62	0.213
2.2	particle-ring no overlap	0.184	0.180	0.254	0.635	0.212
2.3	Z=1	0.161	0.159	0.213	0.572	0.183
2.4	quality of ring	0.172	0.172	0.233	0.604	0.197
2.5	unused RICH hits	0.121	0.119	0.162	0.324	0.142
2.6a	$\beta_{\text{RICH}} < 0.99$	0.114	0.114	0.158	0.033	0.129
2.6b	compatib with TOF	0.181	0.179	0.242	0.631	0.208
2.7a	$\text{E}_{\text{TOF}}^{3,4} < 4\text{MeV}^*$	0.819	0.835	0.927	0.979	0.930
2.7b	no extra TOF3,4 clusters*	0.875	0.875	0.871	0.824	0.900
2	β_{RICH} reconstruction (2.0 $\rightarrow$ 2.7b)	0.052	0.051	0.067	$2 \cdot 10^{-3}$	0.058
5	β reconstruction (1 or 2)	0.347	0.351	0.269	$2 \cdot 10^{-3}$	0.305
		TRK				
3.1	$\text{N}_{\text{hit}} > 5$	0.931	0.932	0.912	0.774	0.919
3.2	$\chi^2_{\text{FastFit}} < 3$	0.851	0.851	0.852	0.819	0.846
3.3	R_{GEANE} compatib.	0.949	0.851	0.971	0.863	0.958
3.4	$\text{p}_{\text{rec}} > 0.85$ GeV/c	0.957	0.955	0.908	0.858	0.891
3.5	$\text{E}_{\text{tunnel}}/\text{E}_{\text{all}} > 0.175$	0.895	0.893	0.862	0.777	0.889
3	p reconstruction	0.643	0.574	0.581	0.388	0.572
		TRD				
4.1	TRD truncated mean	0.900	0.891	0.877	0.035	0.861
4.2	$E_{TRD}^{track}/E_{TRD}^{total} > 0.85$	0.902	0.895	0.878	0.876	0.893
4.3	TRD-TRK track distance	0.937	0.932	0.905	0.898	0.903
6	all cuts (5 & 3 & 4.1-4.3)	0.198	0.181	0.126	$4 \cdot 10^{-5}$	0.132
7	+ mass window cut	0.998	0.990	$4 \cdot 10^{-4}$	< 0.01	$2 \cdot 10^{-4}$
8	final efficiency	**0.198**	**0.180**	$\mathbf{3 \cdot 10^{-4}}$	$\mathbf{< 4 \cdot 10^{-7}}$	$\mathbf{2 \cdot 10^{-4}}$

algorithm is more sensitive in low energy region. This is a good feature from point of view of Dark Matter searches (see Figure 1). The dip in sensitivity for kinetic energy between 1 and 3 GeV/nucleon corresponds to transition between the two detectors used for velocity measurement in TOF and RICH.

In case of **proton** background, the overall efficiency is about $3 \cdot 10^{-5}$, not including the efficiency of misdetermination of the sign of charge. Assuming the sign of charge misidentification efficiency of about 10^{-8}, the further reduction to $3 \cdot 10^{-13}$ can be achieved. Therefore the contribution of proton background reaches negligible level below the signal.

The efficiency of the sign of charge confusion in case of **deuterons** is lower than in the case of protons because of their higher mass. However it is not know precisely how much lower it is. Making a pessimistic assumption that in case of deuterons the sign of charge is mistaken as often as for protons, the deuteron background is reduced to the level of antideuteron signal.
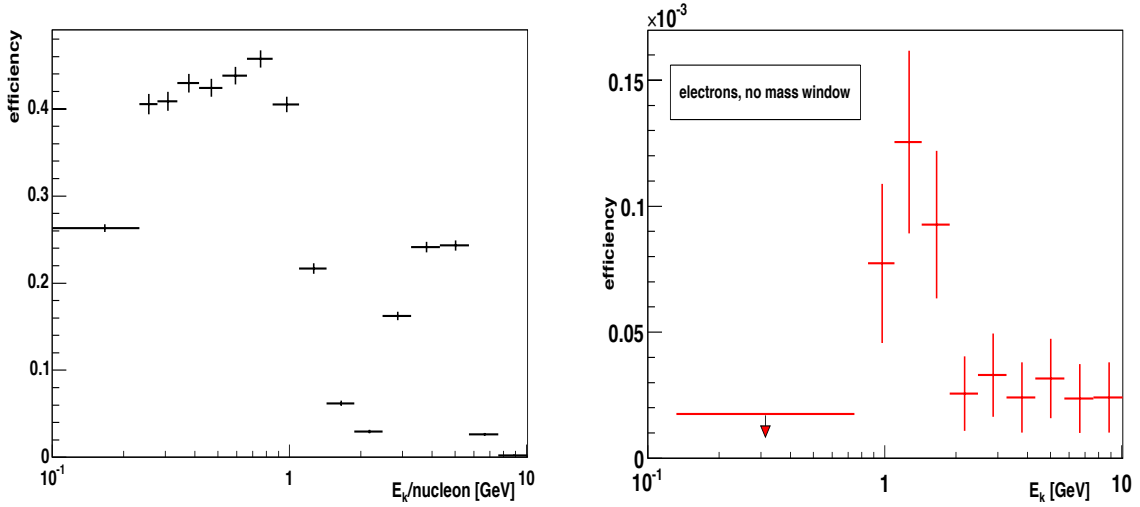
Figure 21: *Efficiency of the selection as a function of particle kinetic energy for antideuterons (left plot) and electrons (right plot). The efficiency for electrons does not include mass window (see discussion in text). For kinetic energies below 1 GeV electrons have momentum too small to go through the magnetic field of Tracker, therefore the efficiency is very low.*

The **electron** background must be reduced by a factor of 10^8. For practical reasons, due to limited statistics available, the electron efficiency has been estimated with an indirect method.

The efficiency of selection as a function of energy, excluding the mass window efficiency, is plotted on the right plot of Figure 21. Electron detection threshold, due

35

to track bending in Tracker magnetic field, is about $E_k = 1$ GeV so the efficiency below that energy is negligible. For kinetic energies between 1 and 2 GeV (TOF measurement range) the efficiency reaches the level of 10^{-4} and for higher energies (RICH measurement range) it is around $2 \cdot 10^{-5}$.

The mass window cut for electrons is illustrated on the left plot of Figure 22. The shape of the reconstructed mass changes with applied selection. The high-mass tail, seen after the preselection (black line), is reduced by the selection requirements (blue line), but the $\beta_{TOF} < \beta_{max}$ requirement (see Section 6.1.4) rejects all disposable statistics. Therefore the mass window rejection factor has been conservatively estimated with use of preselected events.

On the right plot of Figure 22 the mass window cut efficiency as a function of β_{max} is presented. The efficiency is of the order of $8 \cdot 10^{-2}$ and does not depend significantly on β_{max} value, what is an argument in favor of use of the same value for a tighten cut.

On the left plot of Figure 23 the efficiency of the mass window cut is plotted as a function of the electron kinetic energy. Low energy electrons have much lower efficiency to fake antideuteron mass.

To get the final electron efficiency the results presented on the right plot of Figure 21 must be multipied by the ones from left plot of Figure 23. It can be concluded that the final efficiency in TOF region (up to $E_k = 2$ GeV) reaches the level better than 10^{-8} and the level of $2 \cdot 10^{-6}$ for high energies (close to 10 GeV). This is enough to reject the electron background.

Antiprotons are the dominant background for the antideuteron search. The efficiency of rejection as a function of the antiproton kinetic energy is presented on the right plot of Figure 23. For energies above 1 GeV/nucleon it reaches level of 10^{-4} what is not enough to reject antiprotons. The low energy part of the antiproton spectrum (below $E_k = 1$ GeV) is rejected efficiently (better than 10^{-6}) by the mass window requirement. The more restrictive selection of β_{max}, as seen on the left plot of Figure 27, does not improve the signal-to-noise ratio.

7.2 Quality of momentum, velocity and mass reconstruction

The quality of the reconstructed momentum and velocity is presented in Figure 24 for antideuterons and in Figure 25 for antiprotons. The black distributions represent events after preselection and the red ones after the final selection.

In case of antideuterons the momentum reconstruction quality is characterized by two imperfections. The first one is the tail between $0.05 < \frac{\text{PMC}-\text{Prec}}{\text{PMC}} < 0.25$. It is caused mainly by low momentum particles which interact in TRD and loose a significant (5-25%) fraction of their energy.

The second imperfection is characterized by 50% momentum loss. It is generated by protons and antiprotons produced in hard interaction of antideuterons in the
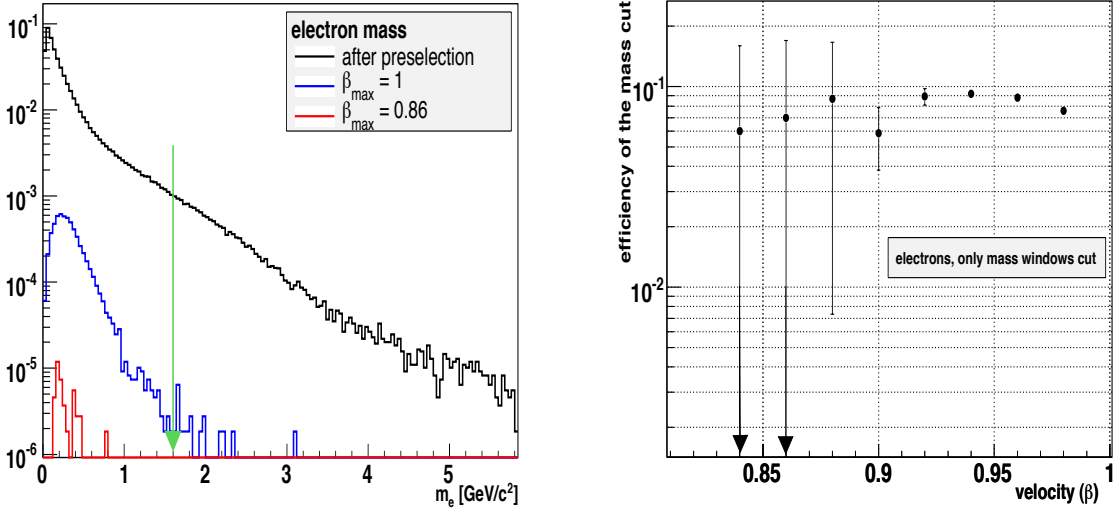
Figure 22: *Left plot presents the electron mass reconstruction: a long tail for high masses is the electron contribution to the background. Black histogram presents reconstructed mass after preselection. The blue histogram is mass after the whole selection chain except of the cut on the maximal velocity measure in TOF (β_{max}) and the red one illustrates the β_{max} selection effect. Right plot presents the efficiency of the mass cut as a function of the cut on β_{max}.*

upstream detectors (TRD, upper TOF). The momentum of these protons is about 50% of the momentum of initial deuterons, so they are visible on the left plot of Figure 24 as a peak for $0.4 < \frac{\text{PMC} - \text{Prec}}{\text{PMC}} < 0.65$. These protons are also visible on the reconstructed mass distribution, on the left plot of Figure 26. The events with overestimated momentum momentum (ie. where $\frac{\text{PMC} - \text{Prec}}{\text{PMC}} < 0$) are almost completely rejected by analysis procedure.

In case of the velocity reconstruction the tail of the distribution of $\frac{\beta_{\text{MC}} - \beta_{\text{rec}}}{\beta_{\text{MC}}}$ which corresponds to overestimated β is reduced mainly by the selection on the maximal value of velocity measured in TOF detector. The tail containing events with underestimated β is reduced mostly by the selections on the quality of TOF reconstruction and by excluding events with interactions in the upstream detectors.

For antiprotons the effects of selections on the final quality of momentum and velocity reconstruction are presented in Figure 25. The momentum and the velocity are reconstructed with less accuracy because antiprotons, as lighter particles, are scattered more than antideuterons. The antiproton events, which remain after the selection have overestimated mass mimicking antideuteron one. They have well reconstructed momentum and slightly underestimated velocity (blue line in Figure 25).

The reconstructed antideuteron and antiproton masses are presented in Figure 26. The black lines represent events after preselection, the red ones after full selection and the blue correspond to the case when velocity is measured by the RICH detector. The

37
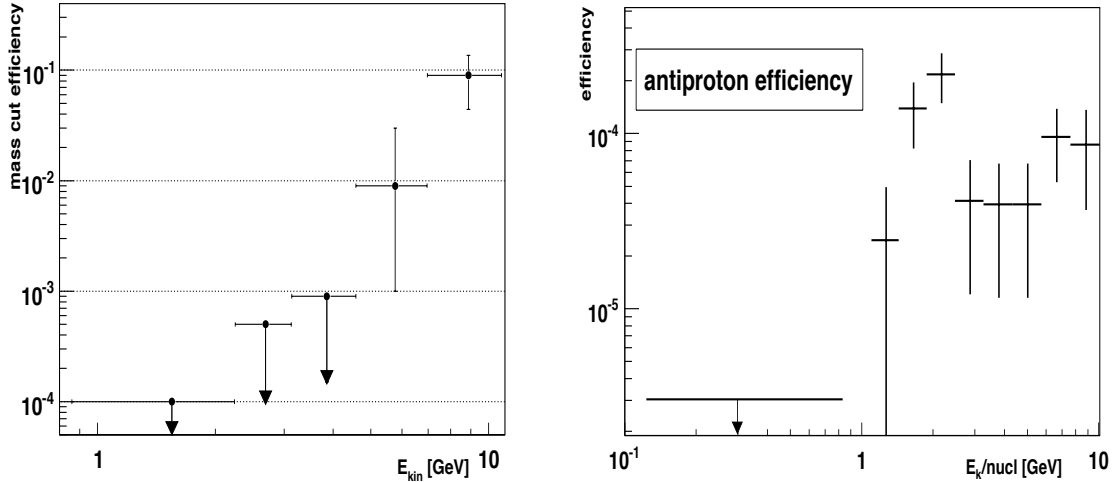
Figure 23: *Efficiency of cuts on mass window for electrons as a function of electron kinetic energy (left plot). Right plot presents the final selection efficiency for antiprotons in function of their kinetic energy. For low energies the efficiency is very small (below reach of statistics).*

green marks indicate the initial point of the antideuteron mass window at $1.6\,\mathrm{GeV/c^2}$.

In conclusion, the absolute mass resolution after selection is better for antiprotons ($0.055\,\mathrm{GeV/c^2}$) than for antideuterons ($0.085\,\mathrm{GeV/c^2}$). The difference is small and σ_m/m is comparable for both types of particles. Unfortunately the tail of antiproton mass distributions extends beyond $1.6\,\mathrm{GeV/c^2}$, constituting an irreducible background for antideuteron search.

7.3 Sensitivity to cosmic antideuterons

In this Section an evaluation of the number of the antideuteron events registered in AMS-02 during three years of data taking on orbit is performed. Two antideuteron sources are considered: spallation (standard) processes, with fluxes of about $10^{-8}[\mathrm{GeV\ m^2\ s\ sr}]^{-1}$ and annihilation of the supersymmetric Dark Matter. An evaluation of antiproton background is performed to estimate the sensitivity of experiment to antideuteron signal.

The procedure takes into account the flux diminution due to the geomagnetic cutoff which is important at the International Space Station altitude. This cutoff reduces the signal and background in low-energy range.
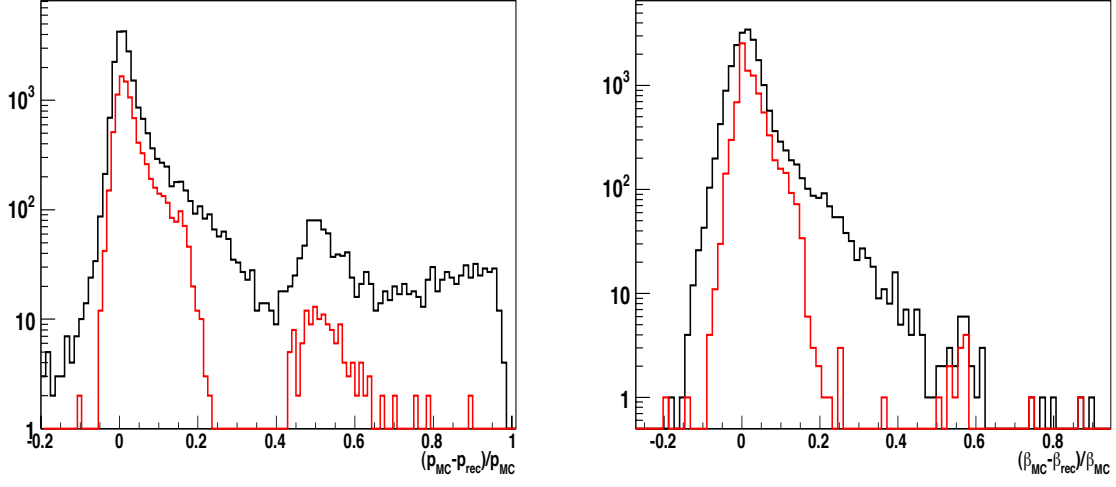
Figure 24: *The quality of the momentum (left plot) and velocity (right plot) recon-struction after preselection (black line) and after all analysis cuts (red line). The sample of antideuterons were used to prepare these plots.*
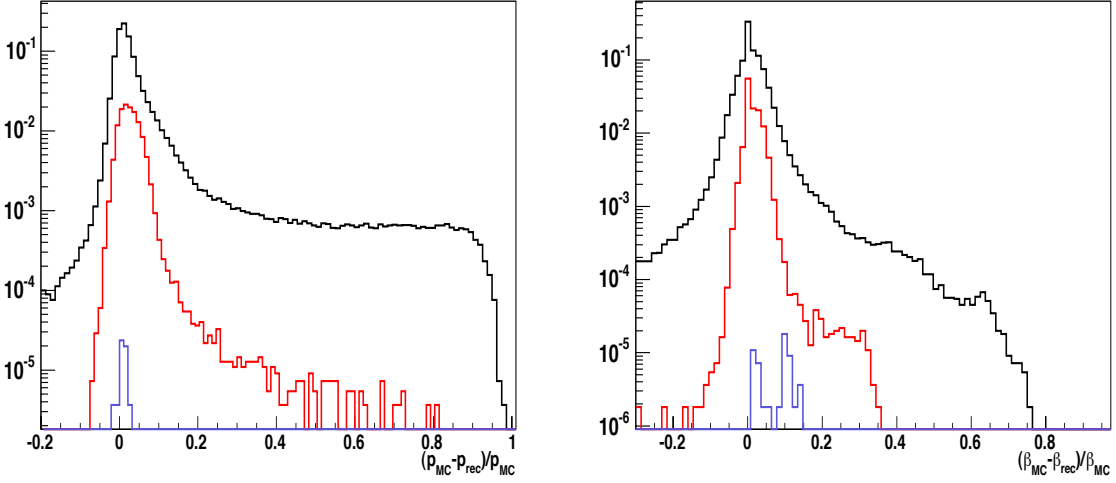
Figure 25: *The quality of the momentum (left plot) and velocity (right plot) recon-struction after preselection (black line), after all analysis cuts (red line) and after mass window cut (blue line). The sample of antiprotons were used to prepare these plots.*

The number of detected antideuterons and antiprotons is given:

$$N = \sum_m \left[t_m \cdot \sum_i \Phi^{\bar{d},\bar{p}}(E_i) A(E_i) \epsilon_i^{\bar{d},\bar{p}} \Delta E_i \right] \tag{9}$$

where the first sum is over the geomagnetic bands (m) and the second one

39
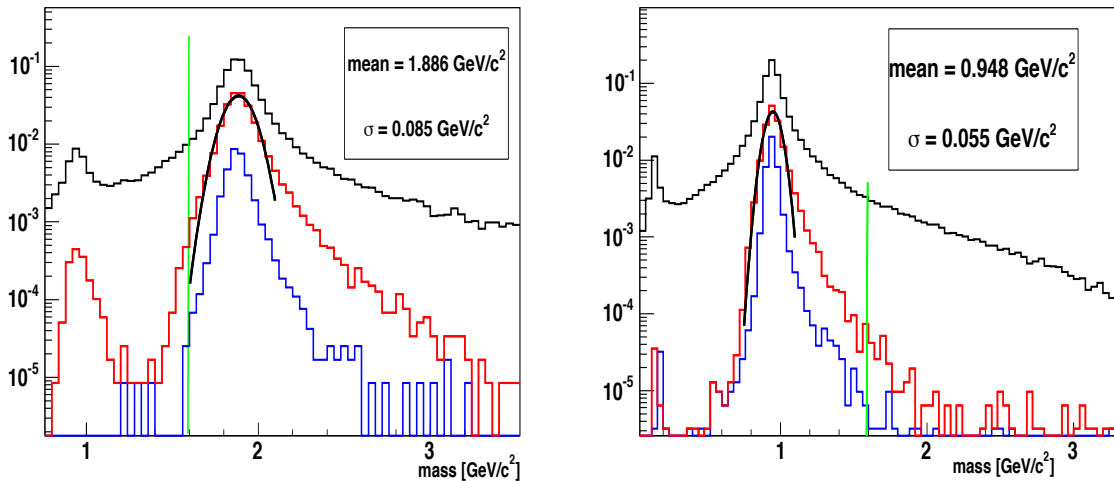
Figure 26: *Left plot: antideuterons mass reconstruction. Black line shows mass distribution after preselection, red one after all cuts and blue one refers to mass when velocity is measured in RICH. Right plot: the same distribution for antiprotons.*

over the kinetic energy bins (i). $\Phi^{\bar{d},\bar{p}}(E_i)$ is the expected differential flux of antideuterons/antiprotons in energy bin i, $A(E_i)$ is the value of the acceptance, t_m is the time the detector spends in a given geomagnetic bin m and $\epsilon_i^{\bar{d},\bar{p}}$ is the analysis efficiency given by the left plot of Figure 21 for antideuterons and by the right plot of Figure 23 for antiprotons.

The calculation is made in 5 geomagnetic bands with geomagnetic cutoff varying from 0.2 GeV/nucleon in the polar region to 2.6 GeV/nucleon in the equatorial one and in 15 bins of kinetic energy.

The antideuteron flux from spallation processes has been evaluated according to [23]. The BESS [24] antiproton flux measurement has been used. In the Figure 27 the approximate expected numbers of antideuteron events (black dots) and antiproton background (red dots) are presented as function of threshold on velocity measurement (β_{max}) in TOF branch of the analysis.

The signal-to-noise ratio reaches 6% for $\beta_{max}^{TRD} = 0.82$ with 4 antideuterons registered during 3 years of AMS-02 flight. In the same time there would be about 60 antiproton events mimicking antideuterons. This background is irreducible due the limited mass resolution, determined by TOF accuracy. Therefore, the significance of the antideuteron detection from the standard spallation processes in AMS-02 is expected to be less than 1σ.

Theoretical estimations of the antideuteron flux vary as the knowledge of the cosmic ray propagation model and cosmic ray sources evolves. Therefore it is important to discuss the AMS-02 sensitivity threshold.

Assuming only antiproton background and a severe cut on velocity measurement

in TOF ($\beta = 0.82$) AMS-02 will be sensitive, at 3 sigma level, to the antideuteron fluxes of about $5 \cdot 10^{-7} - 10^{-6} [\text{m}^2 \text{ s sr GeV}]^{-1}$ (the prediction from [23] is more optymistic and gives the detection threshold of $10^{-8} - 10^{-7} [\text{m}^2 \text{ s sr GeV}]^{-1}$). It means that AMS-02 will be sensitive to $\bar{\text{d}}$ fluxes 5-50 times larger than the ones calculated for the standard production (spallation).
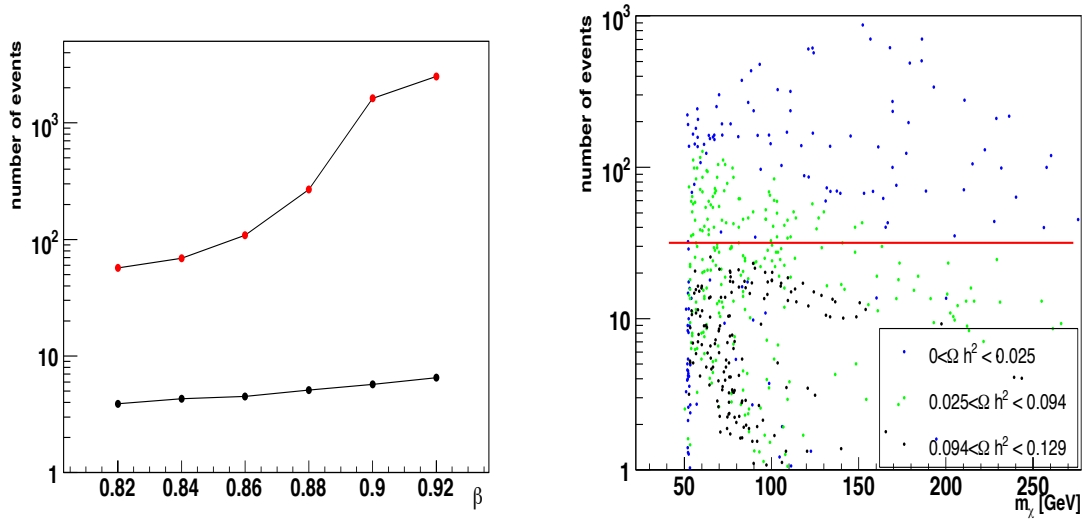
Figure 27: *Left plot: expected numbers of antideuteron events from spallation and antiproton events interpreted as a background to antideuteron search in AMS-02 in function of the cut on the velocity in TOF. Right plot: AMS-02 sensitivity for detection of antideuterons from some supersymmetric models as a function of neutralino mass. NFW halo profile parametrization with the standard set of parameters was used together with boost factor 1000. Colors of marks represent various ranges of Ωh^2, which correspond to models where supersymmetric Dark Matter is a total or a fraction of Dark Matter. Models above the red line are within AMS sensitivity.*

Therefore, if exists an additional source of antideuterons in cosmic rays, a detection in AMS-02 is still possible. An example of such an exotic source is neutralino annihilation which might lead to a significant enhancement of the antideuteron flux. The spectrum of these antideuterons is soft, as mentioned in Section 1.

A generation of 15 thousands of supersymmetric models has been done with use of DarkSUSY 4.1 package [8] interfaced with SUSPECT [9] code. The models are in the range where $0.0 < \Omega_\chi h^2 < 0.129$. The values below the lower WMAP constraint (0.094) [25] belong to additional, non-thermal neutralino production scenarios.

The ranges of the mSUGRA parameters used in simulation were:

$$\text{sign } \mu = \pm 1$$
$$50. \leq m_0 \leq 3000.$$
$$50. \leq m_{1/2} \leq 1600.$$
$$0.1 \leq |A_0| \leq 2000.$$
$$3. \leq tan\beta \leq 60.$$

Unphysical models are excluded from the simulation. The resulting antideuteron flux has been multiplied by a boost factor of 1000, which is a possible boost factor in case of presence of a strong clump within a few parsec from Earth. The amount of detected antideuterons are presented on the right plot of Figure 27. After confronting these numbers with the antiproton background it can be concluded that all the models which lead to detection of 30 or more $\bar{\text{d}}$ events will be visible in AMS-02 with 3σ level (red line).

Naturally the models which foresee a smaller $\Omega_\chi h^2$ give higher fluxes, as they usually foresee higher rate of annihilation. Similar behavior is observed in case of γ-ray signal from Galactic Center [26].

8 Conclusions

In the data collected by AMS-02 during 3-year flight a few (1 to 10) cosmic ray antideuterons originating from standard processes could be identified. In the current configuration the antiproton background cannot be sufficiently reduced. The sensitivity for identification of the light isotopes is constrained by a limited resolution on velocity measurement and by acceptance. More significant results request an improvement in sensitivity by a factor of 100.

Different perspectives are presented for antideuterons produced in neutralino annihilation. There exists a group of Supersymmetric models where cross section for annihilation into antideuterons is large. In addition, the flux of antideuterons is enhanced if Dark Matter halo has a clumpy structure. In case of existence of a dense clump in Earth vicinity its detection with use of antideuteron signal in AMS-02 will be possible.

References

[1] H. Fuke et al. Search for cosmic-ray antideuteron with the bess spectrometer. Prepared for 28th International Cosmic Ray Conferences (ICRC 2003), Tsukuba, Japan, 31 Jul - 7 Aug 2003.

[2] R. Henning. *Search for the Antideuterons and Strangelets in Cosmic Rays with AMS-01*. PhD thesis, Massachusetts Institute of Technology, 2003.

[3] Hideyuki Fuke et al. Search for cosmic-ray antideuterons. *Phys. Rev. Lett.*, 95:081101, 2005.

[4] P. Salati, F. Donato, and N. Fornengo. Cosmic-ray antideuterons as a signature for neutralino annihilation in the galactic halo. *Nucl. Phys. Proc. Suppl.*, 81:37–40, 2000.

[5] Manuel Drees. An introduction to supersymmetry. 1996.

[6] M. Battaglia et al. Updated post-WMAP benchmarks for supersymmetry. *Eur. Phys. J.*, C33:273–296, 2004.

[7] J.F. Navarro, C.S. Frenk, and S.D.M. White. *Astrophys.J.*, 462:563–575, 1996.

[8] `http://www.physto.se/~edsjo/darksusy/`.

[9] G. Moultaka A. Doujadi, J.-L. Kneur.

[10] R. Brun, R. Hagelberg, M. Hansroul, and J. C. Lassalle. Geant: Simulation program for particle physics experiments. User guide and reference manual. CERN-DD-78-2-REV.

[11] F. Giovacchini. private communication, 2006.

[12] V.Choutko. `http://ams.cern.ch/AMS/Analysis/hpl3itp1/ams02_lvl1.ps`.

[13] G. Lamanna. *Measurement of Cosmic Ray Protons and Deuterons spectra in Low Earth Orbit with the Alpha Magnetic Spectrometer (AMS)*. PhD thesis, Perugia University, 2000.

[14] F.Piron. Predictions of grb detection in ams from batse catalog extrapolations. AMS Workshop on sources and GRBs, Montpellier 2002.

[15] L. Brocco et al. The time of flight system of the AMS-02 space experiment. 2001.

[16] C.Delgado. private communication, 2005.

[17] F.Barao R.Pereira. private communication, 2006.

[18] F.Barao R.Pereira. AMS note prepared for publication, 2006.

[19] D. Carafini. *Anti-Proton Flux Detection and Indirect Search for Dark Matter with the AMS-02 experiment.* PhD thesis, Perugia University, 2003.

[20] J. Alcaraz. The alternative track fitting method for AMS. 2003. AMS note 2003-01-02.

[21] E. Nagy V. Innocente, M. Maire. Geane : average tracking and error propagation package. CERN writeup W5013, 1994.

[22] J. C. Hart and D. H. Saxon. Track and vertex fitting in an inhomogeneous magnetic field. *Nucl. Instr. Meth.*, A220:309–326, 1984.

[23] R. Duperray et al. Flux of light antimatter nuclei near earth, induced by cosmic rays in the galaxy and in the atmosphere. *Phys. Rev.*, D71:083013, 2005.

[24] J.W. Mitchell et al. Precise measurements of the cosmic ray antiproton spectrum with BESS including the effects of solar modulation. *Adv. Space Res.*, 35:135, 2005.

[25] C. L. Bennett et al. First Year Wilkinson Microwave Anisotropy Probe (WMAP) observations: Preliminary maps and basic results. *Astrophys. J. Suppl.*, 148:1, 2003.

[26] Agnieszka Jacholkowska et al. Indirect dark matter search with diffuse gamma rays from the galactic center with the alpha magnetic spectrometer. *Phys. Rev.*, D74:023518, 2006.